

December 13, 2019

Re.: Revised manuscript “Unexpected long-range transport of glyoxal and formaldehyde observed from the Copernicus Sentinel-5 Precursor satellite during the 2018 Canadian wildfires”.

Dear Dr. McLaren,

we would like to take the opportunity to thank you again for accepting the editorship of our manuscript “**Unexpected long-range transport of glyoxal and formaldehyde observed from the Copernicus Sentinel-5 Precursor satellite during the 2018 Canadian wildfires**”.

We noticed a small mistake in the discussion manuscript. For the AMF calculation in the CHO.CHO and HCHO satellite retrievals, we accidentally used wrong units in the profiles used for the simulations, which created some background offset between different days. In the revised manuscript, we corrected the CHO.CHO and HCHO VCDs. This introduces only relatively small changes in the magnitude of CHO.CHO and HCHO compared to the dataset shown in the discussion manuscript and thus not affect the interpretation of the results.

Please find attached a revised version of our manuscript, the answers to the referees, as well as the manuscript with color-coded changes showing the differences to the original version. We have answered point by point the comments and suggestions of each referee.

We hope that with the submission of the author comments and the revision of the manuscript, our article will be accepted for publication in ACP.

If possible, we would also like to ask to include this manuscript in the TROPOMI special issue (https://www.atmos-chem-phys.net/special_issue400_1002.html)

Yours sincerely,

Leonardo Alvarado (on behalf of the co-authors)

List of attachments:

- Author comments to Referee #1
- Author comments to Referee #2
- Revised manuscript with highlighted changes (color-coded)
- Revised manuscript

Author reply to comments of anonymous Referee #1 on the manuscript
“Unexpected long-range transport of glyoxal and formaldehyde observed from the
Copernicus Sentinel-5 Precursor satellite during the 2018 Canadian wildfires”

Leonardo M. A. Alvarado et al.
December 13, 2019

We would like to thank the anonymous referee #1 for carefully reading our manuscript and providing valuable comments, which helped to improve the quality of our manuscript. We have answered below point by point to each comment.

We noticed a small mistake in the discussion manuscript. For the AMF calculation in the CHO.CHO and HCHO satellite retrievals, we accidentally used wrong units in the profiles used for the simulations, which created some background offset between different days. In the revised manuscript, we corrected the CHO.CHO and HCHO VCDs. This introduces only relatively small changes in the magnitude of CHO.CHO and HCHO compared to the dataset shown in the discussion manuscript and thus does not affect the interpretation of the results.

Legend:

- referee comments
- authors comments

This paper presents satellite-derived observations of glyoxal and formaldehyde from the TROPOMI instrument, over British Columbia, Canada. Elevated column densities were associated with fire hot-spots and observed over distances of up to 1500 km. Based on comparisons with FLEXPART simulations with different lifetimes, effective lifetimes of >20 hours are required to explain the observations. The authors indicate that the effective lifetimes are in contrast to the shorter expected lifetimes of these species.

My main concern with the paper is with the references to the lifetimes of glyoxal and formaldehyde. The paper does not provide adequate evidence to support the determination of atmospheric lifetimes, mainly because chemistry and deposition are not considered (and as the authors state, not within the scope of this paper). The observations of glyoxal and formaldehyde enhancements downwind of the fire hot spots are likely due to formation (and loss) processes (as the authors also note) and thus, reference to lifetimes accounting only for transport time is not appropriate.

We agree that full chemical simulations along the trajectory would enhance our understanding of the chemical transformation taking place as the fire emissions are transported. However, we consider the focus of this study was slightly different. We present simultaneous observations of CHO.CHO, HCHO, NO₂ and CO in plumes coming from wildfires. The FLEXPART simulations describe how the air masses are physically transported from the source of production, in this case, the fires. They are coupled with estimates of the lifetime of a theoretical tracer species travelling in the transported air mass. Our initial assumption, that the formaldehyde and glyoxal were produced

in the fire and then transported and chemically removed, primarily by photolysis and reaction with hydroxyl radicals, clearly does not explain the observed formaldehyde and glyoxal temporal evolution. We consider that FLEXPART simulations provide an important piece of information to help us understand the behaviour of air mass plumes, as they are transported. To avoid confusion we have clarified in the text the objectives of the modelling and our use of the term “effective lifetime” in this study.

This is a relevant paper for ACP and would be of interest to ACP readers. The paper is comprehensive, well written with clear study objectives, logically presented and articulated conclusions. The satellite-derived observations of glyoxal and formaldehyde far downwind of the fire sources are quite interesting and can stand on their own without comparison to ‘expected’ lifetimes.

I recommend acceptance to ACP after addressing the above comments and a few minor comments below.

Thank you very much for your positive comments.

L42: biomass burning includes wildfires – what is meant by indicating both?

The sentence has been removed. What we intended to express here is that pyrogenic emissions include wildfires and agricultural fires.

L49: transported to ‘those’ regions – please clarify or reword
Done

Intro – break into paragraphs for easier reading
Done

L117 – any comment on the uncertainty associated with using an aerosol profile to depict the glyoxal profile?

Quantification of uncertainty associated with the assumed profile is difficult as it depends on several factors such as the geometry of observation, the presence of clouds, the altitude of aerosols, the surface albedo, etc. For this study, we consider that the most accurate approach is assuming a vertical distribution of glyoxal similar to the one measured for the aerosols. This is because no significant contribution from other sources is expected. If there is any contribution from layers close to the ground, it is shielded by the aerosol layers and difficult to detect by satellite under the conditions of the measurements in our case study. This is because the measurement sensitivity decreases below the aerosol layer as most photons are scattered back to the satellite before they can reach these altitudes (Leitao et al., 2010). Here, a sensitivity study has been conducted assuming glyoxal profiles at different altitudes and evaluating the impact on the glyoxal AMFs. Figure 1A shows glyoxal profiles with maximum concentrations at different altitudes. Figure 1B shows the AMFs dependence with SZA for different profiles. All AMFs behave quite similar, however, for layers at higher altitude the AMFs are larger than those for a layer closer to the ground. Relative differences between AMFs were also computed using as reference the profile with maximum concentration at 2 km. The AMFs vary between 15% and 30% for small SZA but larger deviations are found for large SZA, especially for profiles with a maximum at high altitude. In

general, uncertainty associated with the assumed vertical profile is one of the most significant sources of error in DOAS retrievals and can lead to uncertainties between 10 and 30% (Boersma et al., 2004; Lerot et al., 2010).

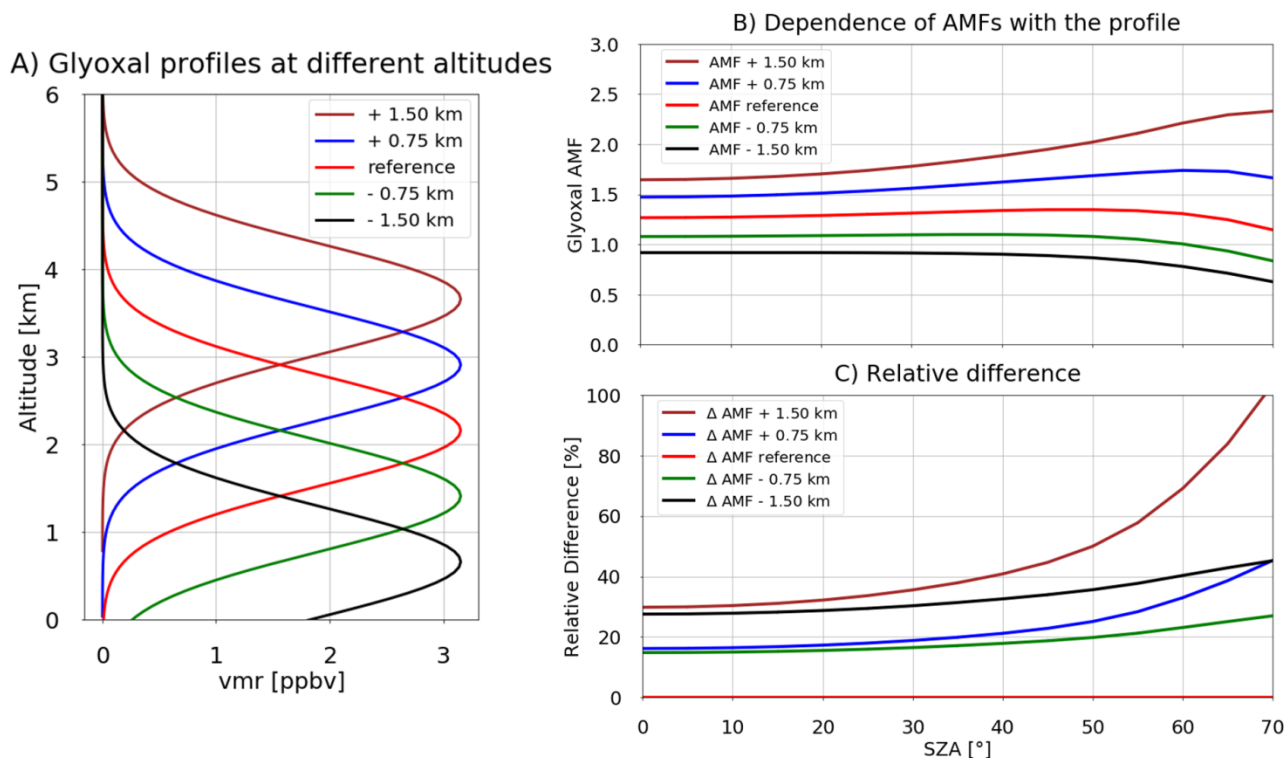


Figure 1: A) Glyoxal profiles peaking at different altitudes. B) Glyoxal AMFs computed using the profiles of A). C) Relative difference of AMFs for profiles at difference altitude against the AMF for the reference profile.

L122 – what is meant by a homogeneous distribution? The same profile is used over the geographic region studied?

Yes is the short answer. We assume that the aerosols are distributed homogeneously in the whole region. For each day, the mean aerosol profile is computed as the average of all aerosol profiles measured in the region after removing cloud-contaminated pixels, and this profile is then used in the retrieval of the trace gas data.

L131 – how much reduction in noise? Can this be quantified?

The random noise in the large fitting range is about 4 times smaller than the corresponding value obtained using a smaller fit window. In the figure below, a comparison of the variation of formaldehyde slant column densities over the equatorial Pacific is shown. In this area, HCHO is mainly produced by methane oxidation and therefore assumed to be homogeneously distributed. Variations in the retrieved HCHO columns are thus taken as indication of retrieval uncertainty. The scatter obtained using a large fitting window corresponds to about 4.5×10^{15} molec.cm⁻², while the fitting window used by Vrekoussis et al., (2010) leads to a variability of about 1.6×10^{16} molec.cm⁻².

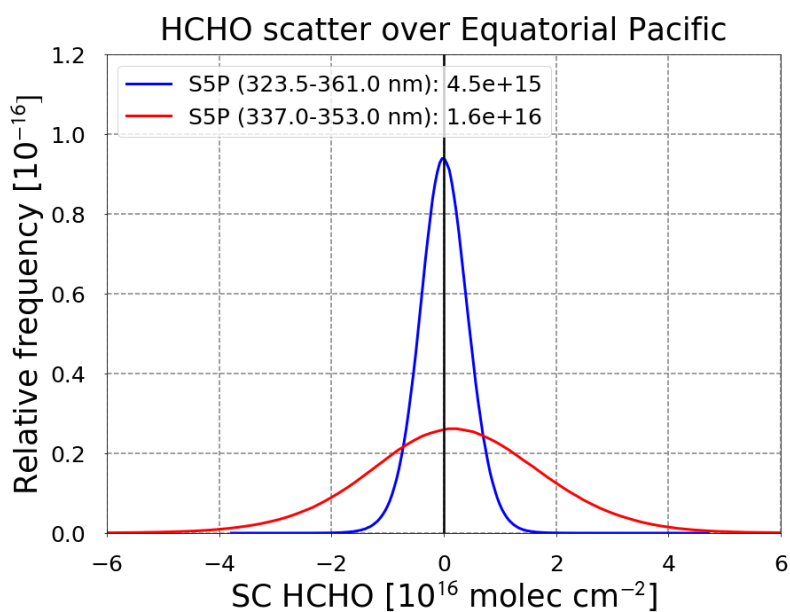


Figure 2: Distribution of S5P HCHO differential slant column densities over a clean equatorial area ocean region (5° S – 5° N, 150° – 210°) for August 2018.

L132 – ‘strong absorption of the latter’; of the latter not appropriate in this sentence, confusing. Remove ‘of the latter’ and clarify.

The manuscript has been modified accordingly.

L150 – confusing sentence regarding lifetimes....

The text has been modified in order to be clearer.

L156 – ‘exact emissions’; what is meant by this? emission type (pollutant?) or emission rate?

Here, we meant “emission rate”, which has been clarified in the revised manuscript.

L161 – reference should be in brackets

Done

References

Leitão, J., Richter, A., Vrekoussis, M., Kokhanovsky, A., Zhang, Q. J., Beekmann, M., and Burrows, J. P.: On the improvement of NO₂ satellite retrievals – aerosol impact on the airmass factors, *Atmos. Meas. Tech.*, 3, 475–493, doi:10.5194/amt-3-475-2010, 2010.

Boersma, K. F., Eskes, H. J., and Brinksma, E. J.: Error analysis for tropospheric NO₂ retrieval from space, *J. Geophys. Res.*, 109, D04311, doi:10.1029/2003JD003962, 2004.

Lerot, C., Stavrakou, T., De Smedt, I., Müller, J.-F., and Van Roozendael, M.: Glyoxal vertical columns from GOME-2 backscattered light measurements and comparisons with a global model, *Atmos. Chem. Phys.*, 10, 12 059–12 072, doi:10.5194/acp-10-12059-2010, 2010.

Vrekoussis, M., Wittrock, F., Richter, A., and Burrows, J. P.: GOME-2 observations of oxygenated VOCs: what can we learn from the ratio glyoxal to formaldehyde on a global scale?, *Atmos. Chem. Phys.*, 10, 10 145–10 160, doi:10.5194/acp-10-10145-2010, 2010.

Author reply to comments of anonymous Referee #2 on the manuscript
“Unexpected long-range transport of glyoxal and formaldehyde observed from the
Copernicus Sentinel-5 Precursor satellite during the 2018 Canadian wildfires”

Leonardo M. A. Alvarado et al.
December 13, 2019

We would like to thank the anonymous referee #2 for carefully reading our manuscript and for providing valuable comments, which helped to improve the quality of our manuscript. We have answered below point by point to each comment.

We noticed a small mistake in the discussion manuscript. For the AMF calculation in the CHO.CHO and HCHO satellite retrievals, we accidentally used wrong units in the profiles used for the simulations, which created some background offset between different days. In the revised manuscript, we corrected the CHO.CHO and HCHO VCDs. This introduces only relatively small changes in the magnitude of CHO.CHO and HCHO compared to the dataset shown in the discussion manuscript and thus not affect the interpretation of the results.

Legend:

- referee comments
- authors comments

This paper describes TROPOMI satellite retrievals of glyoxal (CHO.CHO) and formaldehyde (HCHO) over Western Canada during the wildfire-intensive month of August 2018. Enhanced VCDs of $\sim 14 \times 10^{14}$ molec cm^{-2} CHO.CHO and $\sim 50 \times 10^{15}$ molec cm^{-2} HCHO are observed at wildfire locations and these enhancements appear to persist over long distances of up to 1500 km. FLEXPART tracer transport simulations using GFAS emission locations are able to reproduce the spatial distribution of enhancements if a lifetime of 20 hours or more is used.

My general suggestion for the paper is to articulate more clearly the usage of lifetimes in FLEXPART to avoid confusion. Since a full chemical transport model is not being used, (1) the model is not producing CHO.CHO and HCHO columns that can be directly compared to the observations and (2) the ‘effective lifetime’ does not represent the chemical/physical production/loss processes that are occurring within the large wildfire plume. Rather, the ‘effective lifetime’ in FLEXPART simply allows tracer particles to persist from their origin and continue to be transported. This provides a general spatial comparison to the observations. Hence the ‘effective lifetime’ here is a simple and useful computational proxy – but not a representation of – complex plume processes. The authors have clarified this in the Methods but it should be made more obvious to readers in other sections.

For example, the wording in the abstract suggests >24 hour lifetimes during night-time or at high latitudes (does this refer to Canadian latitudes?) and presents 20+ hours as the FLEXPART lifetime; these are referring to the different usages described above and can be confusing.

The authors discuss the far downwind CHO.CHO and HCHO observations and suggest continued production from precursors as the likely cause, and not a physical increase in the lifetimes. It is worth noting that British Columbia is a coastal province and the presence of chlorine-initiated oxidation adds to the skepticism of >20 hr lifetimes.

We thank the reviewer for the comment. We agree that this study does not try to determine the current chemical lifetimes of these species, and the simulations are only used to describe how they are physically transported from the source of production. The estimated lifetime over which these species are observed in the atmosphere corresponds to the assumption of a simple exponential first-order decay which is not representative for the complex chemistry in the plume. We have clarified in the text what we mean by this effective lifetime in our study to avoid confusion. However, we believe that FLEXPART simulations provide an important piece of information for understanding the behaviour of the plume until it is dispersed.

Regarding the latitudes in the manuscript, these refer to Canadian latitudes. The lifetimes of VOC depend on the season and these are connected to OH variability, and thus to photolysis as well. Globally, OH significantly decreases for latitudes larger than 45°N (Lelieveld et al., 2016), which corresponds to Canadian latitudes, and thus we expect longer lifetimes for VOCs over these latitudes.

This is a relevant paper for ACP. The paper is well written and the results are presented in an organized manner. The satellite retrievals of CHO.CHO and HCHO from the recently launched TROPOMI instrument are highly valuable and provide improved insight into Canadian wildfires as presented in this work. I recommend acceptance to ACP after addressing the above comments and the minor corrections below:

Thank you very much for your positive comments.

Line 05 – ‘lifetimes’

Done

Line 24 – order of CHO and HCHO is awkwardly changed in this sentence

It has been rearranged in the revised manuscript.

Line 51 – remove comma after ‘Spectroscopy’

Done

Line 57 – remove comma after ‘07’

Done

Line 73 – ‘and/or’

Done

Line 81 – capitalize ‘Precursor’ and remove ‘of’

Done

Line 85 – remove ‘of’

Done

Line 86 – keep formatting of dates consistent (e.g. 13 October 2017 vs. August 07 2018 in Line 57 vs. 10th of August 2018 in Line 140, etc.)

The text has been modified in order to be consistent.

Line 89 – 13:30 LT

The manuscript has been modified accordingly.

Line 92 – again consider removing ‘of’

Done

Line 94/95 – keep formatting of in-text citations consistent

The manuscript has been modified accordingly.

Line 106 – How many CHO.CHO peaks are within this range?

In the fitting range used in this study, five glyoxal absorption peaks can be found (see Figure 2A in the manuscript), including the strongest absorption band of glyoxal.

Line 110 – What is meant by a ‘row-dependant’ spectrum? Explain. Is it one background spectrum per line of latitude? The author states that a daily mean is used but if the background spectrum changes throughout the day, will this introduce significant error?

Here, a daily background spectrum is computed by averaging over the whole latitude range (50° S – 50° N) for each across-track viewing direction individually. Thus, one background spectrum is used per viewing direction (450 spectra). This approach is taken to minimise small across-track dependent differences of the TROPOMI measurements.

Ideally, a solar irradiance measurement would be used as a background spectrum in the analysis. However, for weak absorbers such as glyoxal and formaldehyde, use of a daily Earth shine background derived by averaging measurements over the Pacific has proven to reduce noise and offsets in the data. Day to day changes of this background spectrum are small and are therefore expected to introduce only small uncertainties. However, over longer time periods (weeks and months), instrumental drift may induce changes in trace gas columns if the background spectrum is not based on recent measurements. Use of a daily background spectrum resulted in a significant reduction of instrumental noise similar to that demonstrated in previous studies (Schönhardt et al. 2008, De Smedt et al., 2008, Anand et al., 2015, Alvarado, 2016).

Line 110 – ‘...as a background spectrum (Alvarado, 2016).’

Done

Table 1 – remove ‘de’ in title

Done

Line 127 – heading should state ‘HCHO retrieval from TROPOMI measurements’ to match Line 93

Done

Line 133 – ‘consists’

Done

Line 161 – full citation in brackets

Done

Line 206 – remove comma

Done

Line 211 – ‘HCHO’

Done

Line 220 – reword to ‘...which are discussed in detail in Section 3.2.’

The manuscript has been reworded accordingly.

Line 229 – reword to ‘Figure 7 presents...’

The manuscript has been reworded accordingly.

Line 231 – ‘However, on the 20th...’

Done

Line 233 – ‘from’

Done

Line 252 – ‘references’

Done

Figure 8 caption – ‘...for the 10th of August 2018.’

Done

Line 286 – misspelling of ‘conclusions’ in heading

This has been corrected in the manuscript.

References

Anand, J. S., Monks, P. S., and Leigh, R. J.: An improved retrieval of tropospheric NO₂ from space over polluted regions using an Earth radiance reference, *Atmos. Meas. Tech.*, 8, 1519–1535, 2015.

Alvarado, L. M. A., Richter, A., Vrekoussis, M., Wittrock, F., Hilboll, A., Schreier, S. F., and Burrows, J. P.: An improved glyoxal retrieval from OMI measurements, *Atmos. Meas. Tech.*, 7, 4133–4150, 2014.

De Smedt, I., Müller, J.-F., Stavrakou, T., van der A, R., Eskes, H., and Van Roozendael, M.: Twelve years of global observations of formaldehyde in the troposphere using GOME and SCIAMACHY sensors, *Atmos. Chem. Phys.*, 8, 4947–4963, 2008.

Lelieveld, J., Gromov, S., Pozzer, A., and Taraborrelli, D.: Global tropospheric hydroxyl distribution, budget and reactivity, *Atmos. Chem. Phys.*, 16, 12477–12493, [acp-16-12477-2016](#), 2016.

Schönhardt, A., Richter, A., Wittrock, F., Kirk, H., Oetjen, H., Roscoe, H. K., and Burrows, J. P.: Observations of iodine monoxide columns from satellite, *Atmos. Chem. Phys.*, 8, 637–653, 2008.

Unexpected long-range transport of glyoxal and formaldehyde observed from the Copernicus Sentinel-5 Precursor satellite during the 2018 Canadian wildfires

Leonardo M. A. Alvarado¹, Andreas Richter¹, Mihalis Vrekoussis^{1,2,4}, Andreas Hilboll¹, Anna B. Kalisz Hedegaard^{3,1}, Oliver Schneising¹, and John P. Burrows¹

¹Institute of Environmental Physics (IUP), University of Bremen, Bremen, Germany

²Center of Marine Environmental Sciences (MARUM), University of Bremen, Bremen, Germany

³Institute of Atmospheric Physics, German Aerospace Center (DLR), Oberpfaffenhofen-Wessling, Germany

⁴Energy, Environment, and Water Research Center, The Cyprus Institute, Nicosia, Cyprus

10 *Correspondence to:* Leonardo M. A. Alvarado (lalvarado@iup.physik.uni-bremen.de)

Abstract. Glyoxal (CHO.CHO) and formaldehyde (HCHO) are intermediate products in the tropospheric oxidation of the majority of ~~V~~olatile ~~e~~Organic ~~e~~Compounds (VOC). CHO.CHO is also a precursor ~~offer of~~ secondary organic aerosol (SOA) ~~formation~~ in the atmosphere. ~~These VOCs~~ CHO.CHO and HCHO are released from biogenic, anthropogenic, and pyrogenic sources. CHO.CHO and HCHO tropospheric lifetimes are typically considered to be short during the daytime ~~and~~ at mid-latitudes (~~fewe.g. several~~ hours), as they are rapidly removed from the atmosphere by their photolysis, oxidation by OH, and uptake on particles ~~/ or~~ deposition. ~~During nighttime~~ At night and ~~or~~ at high latitudes, ~~lifetime can be prolonged~~ tropospheric lifetimes increase to many hours or even days. Previous studies demonstrated that CHO.CHO and HCHO ~~can be~~ vertical column densities, VCDs, are well retrieved from space-borne observations using the ~~DOAS method~~ differential optical absorption spectroscopy, DOAS. In this study, we present CHO.CHO and HCHO ~~columns~~ VCDs retrieved from measurements of the TROPOMI instrument, launched ~~recently~~ on the Sentinel-5 Precursor (S5P) platform in October 2017. ~~Strongly~~ We observed strongly elevated amounts of CHO.CHO and HCHO ~~are observed~~ during the 2018 fire season in British Columbia, Canada, where a large number of fires occurred in August ~~2018~~. CHO.CHO and HCHO plumes from individual fire hot-spots are observed in air masses travelling over distances of up to 1500 km, i.e. much longer than expected for the relatively short ~~atmospheric~~ tropospheric lifetime ~~of expected for~~ CHO.CHO and HCHO. ~~However, the temporal evolution of the plume differs for both species.~~ Comparison with ~~Lagrangian-based FLEXPART~~ simulations ~~for particles with different lifetimes shows~~ by the particle dispersion model FLEXPART indicates that effective lifetimes of 20 hours and more are needed to explain the observations, ~~indicating that~~ of CHO.CHO and HCHO if they decay in an effective first order process. FLEXPART used in the study calculates accurately the transport. In addition an constant exponential decay, in our case assumed to be photochemical, of a species along the trajectory is added. We have used this simple approach to test our assumption that the CHO.CHO and HCHO are created in the fires and then decay at a

constant rate in the plume, as it is transported. This is clearly not the case and we infer that- CHOCHO and HCHO are either efficiently recycled during transport, or, continuously formed from the oxidation of longer-lived precursors present in the plume, or possibly a mixture of both. We consider the best explanation of the observed CHO.CHO and HCHO VCD in the plumes of the fire is that they are either efficiently recycled during transport or, continuously formed from the- produced by oxidation of -longer-lived precursors, also released by the fire and present in the plume.

1 Introduction

Formaldehyde (HCHO) is produced in the oxidation of both methane (CH_4) and other Volatile Organic Compounds (VOC). Glyoxal (CHO.CHO) is the smallest alpha-dicarbonyl formed in the oxidation of ~~most~~many VOC containing two or more carbon atoms. Although both ~~HCHO and~~CHO.CHO ~~and~~ HCHO, which are known as OVOC (Oxygenated Volatile Organic Compounds) have similar rates of reaction with the hydroxyl radical (OH) in the troposphere, the photolysis frequency of HCHO, which absorbs and is photolysed in the ultraviolet-A (UV-A), is significantly smaller than that of CHO.CHO, which absorbs in the blue. As a result, the atmospheric lifetime of HCHO is longer than that of CHO.CHO (Atkinson, 2000). Both species are short-lived during daytime due to their rapid removal by photolysis and reaction with OH radicals (Atkinson, 2000; Volkamer et al., 2007). These processes are the major sinks of CHO.CHO and HCHO, contributing about 69% and 96%, respectively. ~~T~~he remaining part of HCHO ~~being~~ is removed by deposition (4%), while for CHO.CHO, 22% are removed by SOA formation and 8% by deposition (Stavrakou et al., 2009a, c). Additionally, HCHO and probably also CHO.CHO during ~~nighttime can also be~~ the night are removed by reaction with nitrate (NO_3) radicals (Atkinson, 2000). ~~HCHO and~~CHO.CHO ~~and~~ HCHO play a key role in tropospheric chemistry because they act as temporary reservoirs ~~of~~ VOC; ~~additionally, they produce~~ -releasing carbon monoxide (CO) and HOx (OH and Hydroperoxyl, HO_2) free radicals, which participate in catalytic cycles creating and destroying tropospheric ozone (O_3).

The slant and vertical column ~~amounts~~densities of HCHO were first observed from space using measurements from the GOME instrument (e.g. Burrows et al., 1999, and references therein). These columns were later used to estimate the emission strength of precursor VOC (Palmer et al., 2003; Abbot et al., 2003). The simultaneous observation of CHO.CHO and HCHO (Wittrock et al., 2006) enabled an improved assessment of atmospheric VOC levels and the knowledge of the ratio of CHO.CHO-to-HCHO (R_{GF}), (Vrekoussis et al., 2010), provides some ~~source~~-differentiation: of source types. Studies have used HCHO, partly in combination with CHO.CHO to estimate the biogenic isoprene emissions (Fu et al., 2007; Stavrakou et al., 2009a, b, c; Liu et al., 2012; Marais et al., 2012). This is the largest natural source of CHO.CHO (Guenther et al., 2006; Fu et al., 2007). The amount of biogenically emitted VOC depends on several factors including, amongamongst others, the plant species and weather -conditions (e.g. temperature and humidity) (Guenther et al., 2000). In ~~industrialized~~ areasurban and rural regions, there are also contributions to the amounts of CHO.CHO from human activities, such as from fossil fuel production, distribution and combustion: the largest anthropogenic source of VOC precursors of CHO.CHO being

motor vehicle emissions due to either evaporation or incomplete combustion of fuel (Kansal, 2009). Globally, 55% of CHO.CHO is produced by biogenic precursors, while 27% are from anthropogenic and the remaining 18% from pyrogenic emissions, ~~which include wildfires and biomass burning (Stavrakou et al., 2009a).~~ (Stavrakou et al., 2009a). Fires and vehicle exhausts are thought to be the only two sources, which directly emit CHO.CHO (Stavrakou et al., 2009a; Zhang et al., 2016).

In August 2018, ~~unusually~~ unusually high temperatures caused severe drought in some areas of North America and resulted in the outbreak of many wildfires: the province of British Columbia (BC) in Canada was one of the most affected areas. The 2018 season ~~has been~~ is the worst on record, with 6826 fires being detected and an area of approximately 22500 km² of land burned (~~Canada, 2018).~~ (Natural Resources Canada, 2018). These fires emitted many different ~~species~~ pollutants into the atmosphere, e.g. CO, NO_x, VOC, OVOC, O₃, SO₂, CO₂, HCHO, HONO, CH₃CO.O₂.NO₂ (PAN) and other toxic species ~~and as well as~~ aerosols (Urbanski et al., 2018). During the transport of plumes from fires, photochemical transformation of emitted species occurs. Overall, ~~pollution resulting in low~~ polluted air ~~quality~~ is transported to ~~those~~ regions where the plumes ~~descend to the surface. HCHO and~~ are dispersed. CHO.CHO and HCHO column amounts are observed by remote sensing from satellite using Differential Optical Absorption Spectroscopy, (DOAS), ~~using~~ on measurements of the radiances backscattered from the Earth's surface and atmosphere. The global maps of ~~the HCHO and~~ CHO.CHO and HCHO retrieved from SCIAMACHY, GOME-2, and OMI show enhanced ~~HCHO and~~ CHO.CHO and HCHO over tropical rain forests but also over other regions with high isoprene emissions. In addition, hot-spots of ~~HCHO CHO.CHO~~ and ~~HCHO CHO.CHO~~ from fire emissions can be detected over large wildfires (Wittrock et al., 2006; Vrekoussis et al., 2009, 2010; Lerot et al., 2010; Chan Miller et al., 2014; Alvarado et al., 2014; De Smedt et al., 2008, 2012, 2015; ~~Smedt et al.~~, 2018).

In this study, we present novel observations of CHO.CHO and HCHO retrieved from the high spatial resolution observations of the instrument TROPOMI on board the S5P platform. On 7 August ~~07~~, 2018, strongly elevated amounts of CHO.CHO and HCHO were observed over British Columbia and attributed to being predominantly from ~~the~~ fires. Surprisingly, these elevated levels of CHO.CHO and HCHO were not limited to the vicinity of the fires. The fire plumes, which contain both CHO.CHO and HCHO remain visible for several days and appear to travel long distances from the sources. We have used forward simulations of atmospheric transport of air masses calculated using the FLEXPART model (~~Pisso et al., 2019a), enable the investigation of long range transport of CHO.CHO and HCHO during the studied period. FLEXPART simulations of a tracer~~ (Pisso et al., 2019). The simulations include an effective first order loss, which determines the mean effective lifetime of the tracer. Those tracers emitted over the fire hot-spots ~~and having with a lifetime of ~29 hours can long~~ effective lifetimes reproduce best the evolution of the plumes of CHO.CHO and HCHO for most of the fire events, and thus provide estimates of the effective lifetimes of CHO.CHO and HCHO in the plumes, as is described in the sections below. ~~In addition,~~ The R_{GF} provides knowledge about their sources in the plume. CO and nitrogen dioxide, NO₂, have respectively longer and shorter lifetimes with respect to reaction with OH, and smoke and aerosol are also transported in the plumes from

fires. Consequently the retrieved vertical column densities of ~~carbon monoxide (CO) retrievals also~~ CO and NO₂ from the TROPOMI instrument and true color images from VIIRS ~~satellite~~ instrument on NPP, which measures near simultaneously with TROPOMI are used as complementary information in ~~order to interpret the~~ our interpretation of the apparent enhanced lifetime of ~~CHO.CHO and HCHO in the plume. Additionally, interpretation of the main source of these species is performed by computing the ratio of CHOCHO to~~ CHO.CHO and HCHO ~~for in~~ the ~~specific events. plume.~~

2 Methods

2.1 CHO.CHO and HCHO observations

The Differential Optical Absorption Spectroscopy (DOAS) method has been successfully applied to retrieve atmospheric columns of trace gases having fingerprint narrow absorption bands in the solar spectral range from space-borne instruments (e.g. Burrows et al., 1999). As noted above, there are several studies describing retrievals of OVOC and their use for the identification of VOC sources ~~emission and their emissions~~ (Burrows et al., 1999; Palmer et al., 2001; Wittrock et al., 2006; Kurosu et al., 2007; Vrekoussis et al., 2009, 2010; Lerot et al., 2010; De Smedt et al., 2008, 2012, 2015, 2018; Hewson et al., 2013; González Abad et al., 2015; Chan Miller et al., 2014; Alvarado et al., 2014, 2015). Algorithms for the retrieval of HCHO and CHO.CHO have been developed for measurements from the SCanning Imaging Absorption spectroMeter for Atmospheric CHartographY (SCIAMACHY) (Burrows et al., 1995; Bovensmann et al., 1999), the Ozone Monitoring Instrument (OMI) (Levelt et al., 2006), and the second Global Ozone Monitoring Experiment on MetOp–A and –B (GOME2–A and–B) (Munro et al., 2016), which in combination provide a continuous dataset covering a period of more than 20 years. In this study, measurements from the TROPOMI instrument on board ~~of~~ the Sentinel–5 ~~p~~Precursor (Veefkind et al., 2012) are used to retrieve atmospheric column amounts of CHO.CHO and HCHO. A brief instrument description and relevant details of the retrieval of CHO.CHO and HCHO are given below.

2.2 The TROPOMI instrument

The TROPospheric Monitoring Instrument (TROPOMI) onboard ~~of~~ the Copernicus Sentinal-5 Precursor satellite was launched on 13 October 2017. It has a spectral range in the UV-VIS-NIR-SWIR covering wavelengths from 270 to 500 nm in the UV- VIS, from 675 to 775 nm in the NIR and in a SWIR band from 2305 to 2385 nm. These bands allow the observation of several relevant atmospheric species, including CHO.CHO, HCHO, NO₂ and CO. TROPOMI provides nearly global coverage each day at a spatial resolution ~~of currently~~ which in August 2018 was 3.5 km×7 km (7 km×7 km in the SWIR). The equator crossing time is 13:00~~30~~ LT (ascending node). Similar to OMI, TROPOMI is a nadir-viewing imaging spectrograph, ~~which consists of~~ employing a two-dimensional CCD, one dimension collecting the spectral information, the other being used for the spatial information. The TROPOMI instrument ~~onboard of~~ on board the S5P satellite provides data since November 2017 (Veefkind et al., 2012).

2.3 CHO.CHO retrieval from TROPOMI measurements

125 In recent years, several improvements on the retrieval of CHO.CHO have been reported. In 2014, Chan Miller et al. (2014)
and Alvarado et al. (2014) presented new CHO.CHO retrieval algorithms applied to OMI measurements. These studies,
similar to previous studies on GOME-2A data, introduced approaches to reduce interference by other absorbers, such as
liquid water and nitrogen dioxide (NO₂). In this study, an optimized retrieval algorithm for CHO.CHO was developed,
building on the heritage from the OMI CHO.CHO retrieval presented by Alvarado et al. (2014), extended and applied to
130 S5P measurements. Previous studies have shown that cross-correlations between references cross-sections, as well as
instrumental structures ~~or features~~ and shifts in the wavelength calibration can introduce systematic errors in the retrieval. As
a result, a strong dependence on the fitting window was identified in the retrieved CHO.CHO slant column densities, SCDs
(Chan Miller et al., 2014; Alvarado et al., 2014). In this study, a fitting window from 433 to 465 nm ~~was~~ chosen, which is
slightly larger than windows used in previous investigations (Vrekoussis et al., 2010; Alvarado et al., 2014). This fitting
135 window, which enables the liquid water absorption to be retrieved, leads to a reduction in the number of negative CHO.CHO
~~SCDs~~ over oceanic regions in comparison to a shorter fitting window (e.g. 434–458 nm), as well as a reduction in the
residuals. The wavelength range selected covers the strong absorption bands of CHO.CHO (452–457 nm), which have
already been used in the past to retrieve CHO.CHO from ground and ship-based DOAS configurations as well as from
satellites (Sinreich et al., 2007, 2010; Wittrock et al., 2006; Vrekoussis et al., 2009, 2010; Lerot et al., 2010; Chan Miller et
140 al., 2014; Alvarado et al., 2014). In order to optimize the quality of the retrievals, a row-dependent daily mean Pacific
spectrum from the region 50°S, 160°E – 50°N, 135°W is used as a background spectrum (Alvarado, 2016), which is
computed by averaging over the whole latitude range (50°S – 50°N) for each across-track viewing direction independently.
In addition, the mean CHO.CHO SCD over the region 30°S, 150°W – 30°N, 150°E is computed each day and subtracted
from all SCDs to correct for possible offsets. A summary of the selected absorption cross-sections, and other parameters
145 used in the retrieval, as well as a list of the species included in the retrieval, is shown in Table 1.

SCDs depend on observation geometry. ~~Vertical column densities (VCDs)~~ are derived from the SCDs by use of so-called air
mass factors (AMFs), which depends on the trace gas profile, ~~air pressure,~~ surface albedo, ~~temperature,~~ aerosols, clouds,
and on solar zenith angle and measurement geometry. As the focus of this study is the observation of CHO.CHO in biomass
burning emissions, a simple CHO.CHO profile with a Gaussian distribution having its maximum peak at the altitude of the
150 aerosol layer is used (see Figure 1-A). This is based on the assumption that CHO.CHO is found at the same location as the
main plume of aerosol and other trace gases. The altitude of the aerosol layer was estimated from profiles retrieved by the
Cloud-Aerosol Lidar and Infrared Pathfinder Satellite Observation (CALIPSO) (Vaughan et al., 2004) (Figure 1-B). These
aerosol extinction coefficients (k_{ext}) profiles retrieved at 532 nm are also used in the calculation of the AMFs by the radiative
transfer model SCIATRAN (Rozanov et al., 2013). The computations have been performed on a daily basis, assuming a
155 single scattering albedo of 0.92 and a homogenous distribution of aerosols characterized by the mean profile in the whole

region of study. The latter is computed from the average of all aerosol profiles, ~~for every single latitude and longitude, and by taken over the region after~~ removing cloud-contaminated pixels (see Figure 1-C). Clouds are not explicitly accounted for in the CHO.CHO and HCHO retrievals but data are filtered for the presence of clouds using an intensity criterion corresponding to a cloud radiance fraction of about 50%.

160

Table 1. Summary of retrieval parameters of CHO.CHO and HCHO ~~de~~ from S5P with the respective absorption cross-sections used.

Parameters	Formaldehyde (HCHO)	Glyoxal (CHO.CHO)
Fitting window	323.5-361 nm	433-465 nm
Polynomial	5 coefficients	5 coefficients
Cross-sections used:		
HCHO (Meller and Mootgat, 2000)	Yes (298 K)	No
CHO.CHO (Volkamer et al., 2005)	No	Yes (296 K)
NO ₂ (Vandaele et al., 1998)	Yes (220 K)	Yes (220K, 2294 K)
O ₄ (Thalman et at., 2013)	Yes (293K)	Yes (293 K)
O ₃ (Serduchenko et al., 2014)	Yes (223 K, 243 K)	Yes (223 K)
BrO (Fleischmann et al., 2004)	Yes (223 K)	No
H ₂ O (Rothman et al., 2013)	No	Yes (296 K)
Liquid water (Mason et al., 2016)	No	Yes (280 K)
Ring effect	Ring cross section calculated by SCIATRAN model (Vountas et al., 1998)	

Non-linear ozone absorption effects, 2 pseudo

absorption cross-sections ($O_3 * \lambda + (O_3)^2$) from Yes

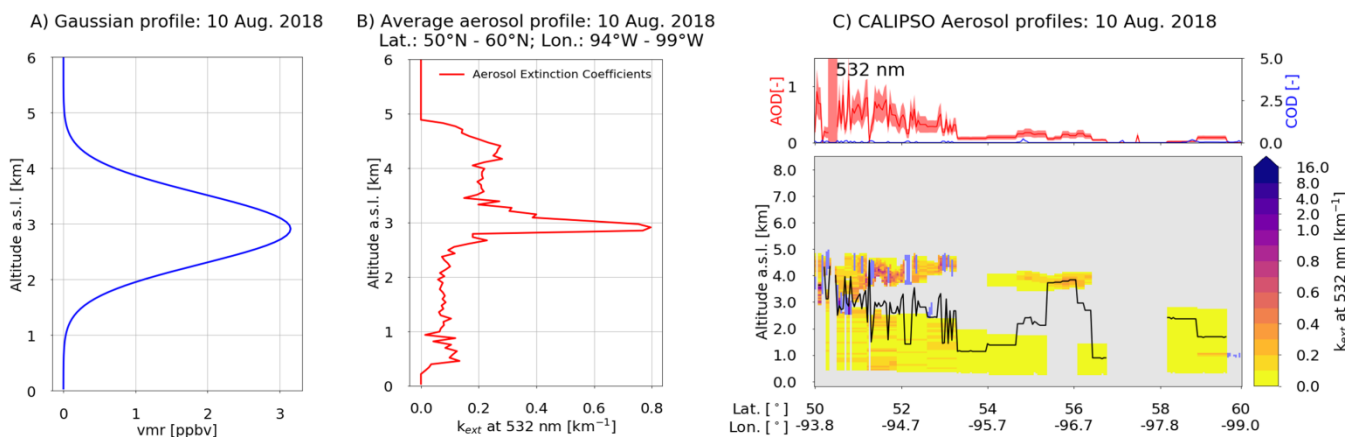
No

Taylor expansion (Pukite et al., 2010)

Iterative spike removal (Richter et al., 2011) Applied

Intensity offset correction Linear offset (I/I0)

Background spectrum Pacific region (50° N, 135° W – 50° S, 160°)



165

Figure 1. A) CHO,CHO and HCHO profiles assumed in the computation of AMFs. B) CALIPSO ~~average~~ profile of aerosol extinction coefficients (k_{ext} , averaged over for all latitudes and longitudes of Figure 1-C, excluding cloudy scenes. C) Top panel: Example of CALIPSO Aerosol profile extinction coefficients retrieved at a wavelength of 532 nm. Aerosol and cloud optical depth are shown as a function of latitude and longitude for every single profile. Bottom panel: Colour coded k_{ext} for every latitude and longitude in the selected region. Purple spots represent cloudy scenes. The black line depicts the aerosol layer height.

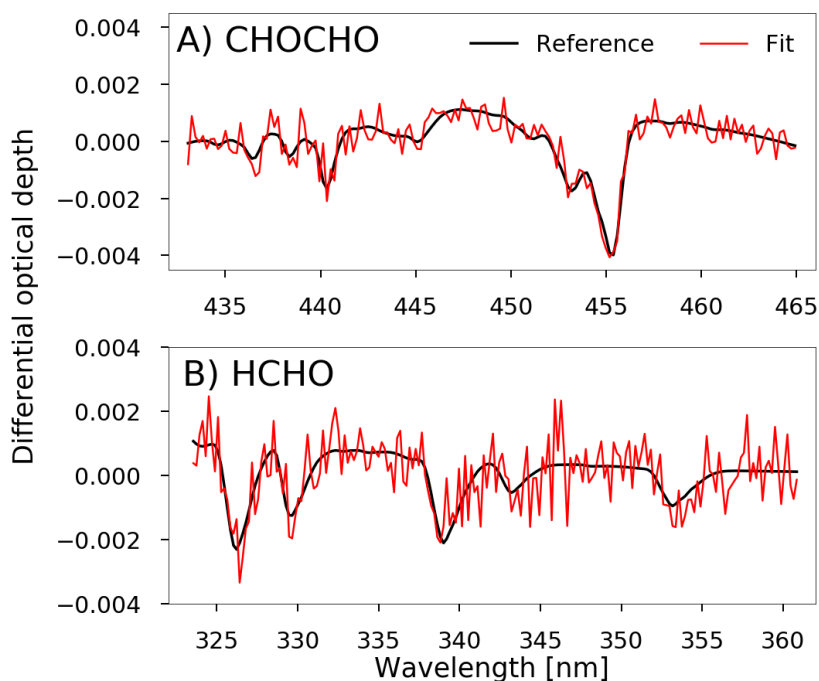
170

2.4 HCHO retrieval from TROPOMI measurements

The accuracy of DOAS retrievals of HCHO is limited by cross-correlations with strong absorbers in the UV (e.g. O_3) and the signal to noise ratio of the radiance spectra measured by the instrument. Here, an updated and optimized version of the formaldehyde retrieval developed by Wittrock et al. (2006) and Vrekoussis et al. (2010) is used, which applies a slightly larger fitting window extending from 323.5 nm to 361 nm, resulting in a reduction in the noise of the retrieved columns.column densities. At wavelengths shorter than 336 nm, interference with O_3 is observed due to the strong absorptionssmall optical depth of ~~the latter~~ HCHO, which is about three orders of magnitude smaller. This effect is compensated by applying the method described by Pukite et al. (2010), which consistconsists of adding two additional pseudo-cross-sections to the fit ($\lambda\sigma_{O_3}$ and $\sigma^2_{O_3}$) (Pukite et al., 2010; De Smedt et al., 2008, 2015, 2015; ~~Smedt et al.~~, 2018).

175

180 The cross-sections of interfering species are included in the fit as listed in Table 1. Similar 1. In a manner similar to glyoxal the retrieval of CHO.CHO, a synthetic ring spectrum (Vountas et al., 1998) is used to account for the Ring effect and a row-dependent daily mean Pacific spectrum from the region 50°S, 135°W – 50°N, 160°E is used as background spectrum. Also, a latitude dependent offset correction based on SCDs from longitudes between 180° E and 160° E is applied to the data. As for CHO.CHO, VCDs_r are computed using AMFs, assuming a Gaussian shape for the distribution of HCHO at the layer where the aerosols are located in the plume. Figures 2-A and 2-B show examples of CHO.CHO and HCHO fit results for the 10th of 10 August 2018, compared to the differential reference cross-section for a single measurement. For an individual CHO.CHO measurement, the detection limit is of the order of 5×10^{14} molec.cm⁻², which is about 10 times smaller than the columns detected from emissions of the wildfires over the British Columbia region of Canada. For HCHO, the detection limit is an order of magnitude higher (54.5×10^{15} molec.cm⁻²). The detection limit of a single S5P measurement in this study has been estimated in a manner similar to that explained in Alvarado et al. (2004).



195 Figure 2. A) Example fit for CHO.CHO from a single measurement of S5P taken at latitude 53.0° and longitude 125.6°W, on the 10th of August 2018 and for a solar zenith angle of 39.3°. B) Example fit for HCHO from a single measurement of S5P taken at latitude 59.1° and longitude 109.0° W, on the 10th of August 2018 and for a solar zenith angle of 44.6°. The black line depicts the scaled differential cross-section and the red line the fit. The SCD values for this example are 9.3×10^{15} molec.cm⁻² for CHO.CHO and 4.6×10^{16} molec.cm⁻² for HCHO, respectively. The detection limit for a single measurement from S5P is estimated to be 5.0×10^{14} molec.cm⁻² and 54.5×10^{15} molec.cm⁻² for CHO.CHO and HCHO, respectively.

2.5 Simulation of tracer transport with FLEXPART

In order to simulate the transport of emissions from the Canadian wildfires, forward simulations with version 10.3 of the FLEXible PARTicle dispersion model FLEXPART (Stohl et al., 2005; Pisso et al., 2019) have been performed. The model was driven by using hourly wind fields from the ECMWF ERA5 reanalysis (C3S) at 0.25° horizontal resolution. As a transport model, FLEXPART ~~cannot adequately~~does not simulate the complete set of chemical transformations leading to the observed lifetimes of trace gases in the biomass burning plumes. ~~Nevertheless~~However, performing simulations for tracers having different mean lifetimes ~~and comparing these to the observed columns~~ yields a valuable ~~insight into the effective lifetime, which the emitted substances have to have in the plume,~~piece of information in order to ~~explain~~understand the observed plume evolution. An effective mean lifetime can be estimated by comparing the observed behaviour of the CHO, CH₂O and HCHO with different FLEXPART simulations of different assumed tracer lifetimes.

In FLEXPART, the ~~mean~~-effective mean lifetime τ of an emitted tracer is treated as exponential decay with a given half-life ($t_{0.5}$); τ can then be calculated according to $\tau = t_{0.5}/\ln(2)$. As part of this study, FLEXPART simulations were carried out with half-life times of 2, 4, 6, 8, 10, 12, 14, 16, 18, and 20 hours, corresponding to effective mean lifetimes of ~2.9, 5.8, 8.7, 11.5, 14.4, 17.3, 20.2, 23.1, 26.0, and 28.9 hours, respectively. As ~~the exact~~ emissions rates from ~~the~~ wildfires are highly uncertain, the emission fluxes from the Canadian wildfires are assumed to be proportional to fire radiative power (FRP, see below for more details). ~~This means that effectively, emissions are prescribed in the model in arbitrary mass units; scaling the individual emission sources with FRP ensures that when aggregating the simulation results from all fires, each fire's relative contribution to the simulated columns is retained, and the results can be compared to the observed columns.~~ The emissions, prescribed in the model, are taken from the Global Fire Assimilation System (GFAS) daily FRP and plume height data (Rémy et al., (2017). Simulations were performed on a daily basis for the period 6-Aug to 23 August 2018. For each day, all fires from the GFAS data, which had an FRP of more than 3 W_tcm^{-2} were gridded to a 0.350° horizontal pattern. The model was then run forward in time for 120 hours, releasing the tracer for the first 24 hours (the full UTC day) from each of the 0.350° grid cells, assuming no temporal variation throughout the day. Vertically, the emissions within the grid cells were evenly distributed over the range of mean altitude of maximum injection heights given by the GFAS data for the respective grid cell. The output of the simulation contains gridded mass concentrations for each time step. Here, a grid with a horizontal resolution of 0.03125° was chosen, to match the resolution of the gridded satellite observations. Hourly output from the simulation was recorded and then vertically integrated to yield simulated tracer columns. In a post-processing step, for one specific mean lifetime, all simulation results (i.e., simulations for all fires on all days) were aggregated into one dataset. While the absolute tracer column density from the model output cannot be simply compared to the measurements, a comparison of the plume patterns and relative distribution between satellite observation and model output gives an indication about the meaningfulness of the prescribed mean lifetime. At this point, the aggregated model output for one effective mean

lifetime consists of hourly latitude-longitude grids of vertical tracer columns throughout the whole study period. For
230 comparison to the satellite observations, the hourly time slice closest to the time of overpass at 53°N was chosen.

3 Results and discussion

During August 2018, a high-temperature anomaly led to the outbreak of many fires in the Canadian Western province of
British Columbia, resulting in the emission of large quantities of particles and traces gases that in turn affected air quality in
the region. As shown in Figure 3-A and -B, the monthly average of CHO.CHO and HCHO vertical columns from S5P show
235 strongly enhanced values over the fire region, suggesting that these fires were a large direct and/or indirect source of
CHO.CHO and HCHO. Surprisingly, the CHO.CHO and HCHO enhancements are not limited to the main fire region but
extend over large parts of Canada, where only a few fires were observed. In order to investigate the sources of CHO.CHO
and HCHO and their distributions, 24-hour assimilation data of fire radiative power from the Global Fire Assimilation
System (Kaiser et al., 2012) are analysed. Briefly, FRP is a measure of outgoing radiant heat from fires, measured in units of
240 $\text{W}\cdot\text{cm}^{-2}$ and retrieved from space by the MODerate resolution Imaging Spectroradiometers (MODIS) on board of Terra and
Aqua satellites (Justice et al., 2002). The assimilated FRP spatially aggregates all valid fire and non-fire observations from
both MODIS instruments onto a horizontal resolution of $0.1^\circ \times 0.1^\circ$ and computes the total FRP sums for each grid bin
(Justice et al., 2002). The FRP is also used as input in the FLEXPART simulation as described in section 2.5 as a proxy for
emission strength. Figure 3-C shows a monthly average FRP map over North America for August 2018.

245

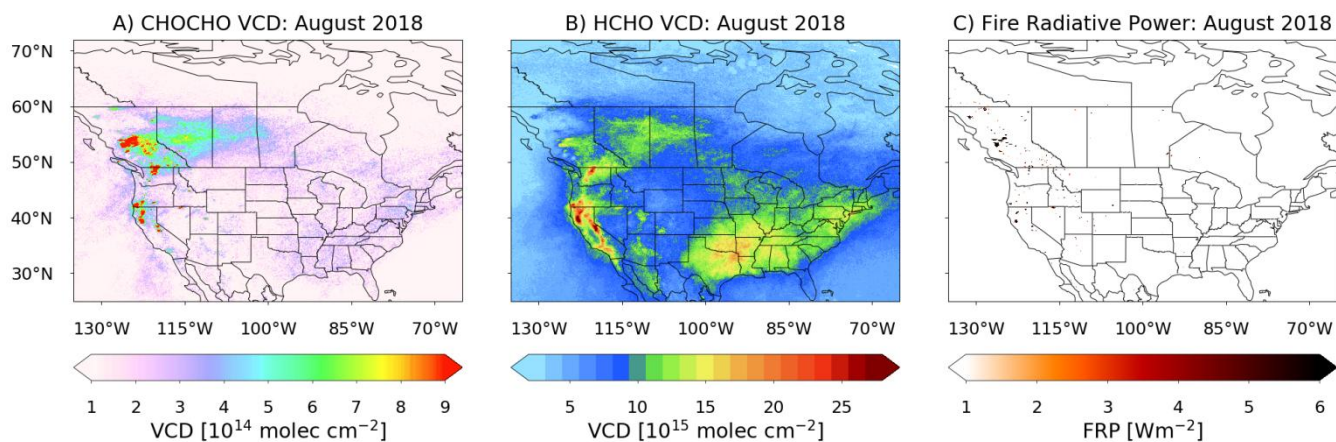


Figure 3. Monthly average of CHO.CHO (panel A) and HCHO (panel B) VCDs retrieved from the TROPOMI instrument on S5P for August 2018, and over North America (A and B). Panel C shows the integrated FRP from MODIS for the same period.

The highest CHO.CHO VCD values are found over the locations of the most intense fires, as intuitively expected. The HCHO distribution over the fire regions is similar to that of CHO.CHO, but with some differences in the relative distribution. In addition, enhanced CHO.CHO and HCHO columns are also apparent over the ~~south-eastern~~southeastern~~south-eastern~~ US, where large isoprene emissions occur. CHO.CHO and HCHO are also detected in plumes crossing central and eastern Canada, where no fires are identified in the FRP map. This pattern ~~points to~~ is best explained by the transport of CHO.CHO and HCHO emanating from the wildfires. However, ~~it is well known that~~ CHO.CHO and HCHO have been reported to have short atmospheric lifetimes of about ~2.2 and ~4.0 hours during daytime, respectively (~~Atkinson, 1998; Volkamer, et al., 2005a~~), which (Atkinson, 2000; Volkamer et al., 2005a). Assuming that the lifetime in the plume is not sufficient similar to ~~explain the~~ that observed ~~pattern at the ground, we expect that CHO.CHO would be removed reasonably close to the fire sources. HCHO would be transported further but we would also expect that it would be transported no more than approximately twice as far as CHO.CHO.~~

Earlier studies by Wittrock et al. (2006) and Vrekoussis et al. (2009, 2010) showed that CHO.CHO is also observed over oceanic regions, where no CHO.CHO source is expected. The potential of a) a long-range transport of CHO.CHO and/or of CHO.CHO precursors from continental areas, and b) having an unknown oceanic CHO.CHO source were discussed as a possible explanation in part of these observations, but no firm conclusions could be drawn so far. In the present study, with the support of the simulations using FLEXPART-model, evidence of long-range transport of CHO.CHO and HCHO or its precursors from biomass burning emissions is ~~shown~~ investigated. In ~~order to further investigate~~ this context the transport of CHO.CHO and HCHO, during two fire plume episodes from different periods ~~of satellite measurements are selected~~ (07-10 and 20-21 ~~of~~ August 2018) ~~and~~ are discussed below.

3.1 CHO.CHO and HCHO emissions from the British Columbia wildfires: 07-10 and 20-21 August 2018

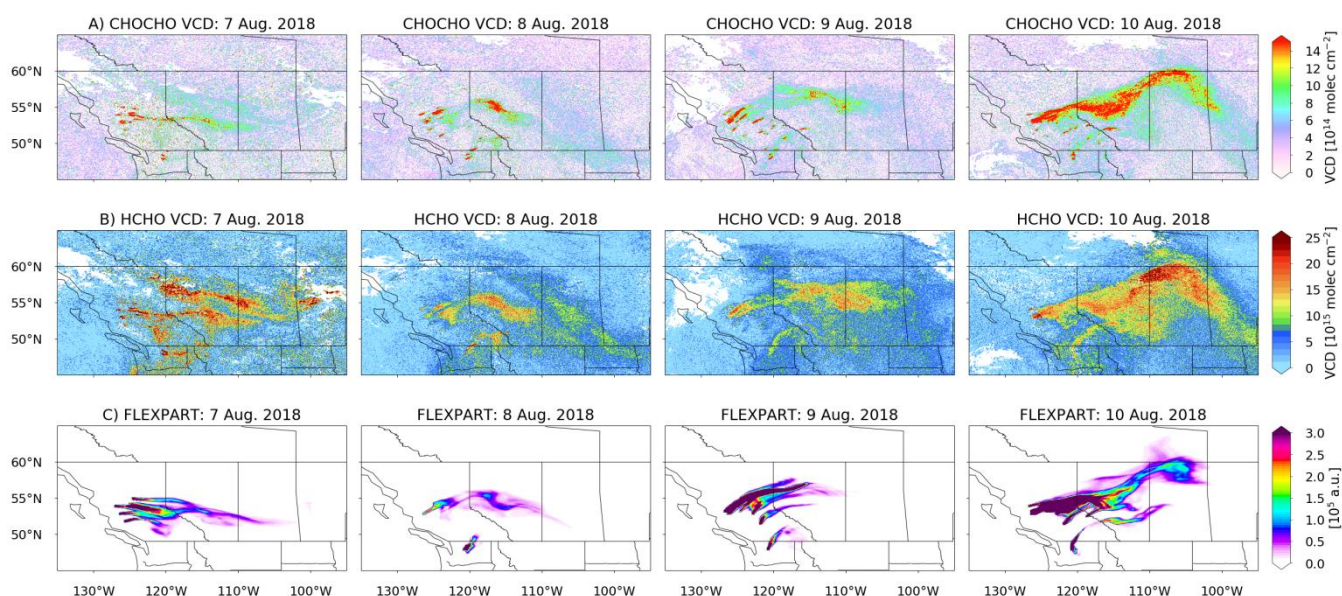
Figure 4-A shows daily maps of CHO.CHO and HCHO VCDs over Canada for the period ~~7th~~ 7 to ~~10th~~ 10 of August 2018. The most intense wildfires are found on ~~the 7th of~~ 7 August 2018 and remain detectable until ~~the 10th of August. The location of those fires corresponds well to the location, where both trace species~~ 10 August 2018. Both CHO.CHO and HCHO plumes are detected on the first day of the fire. The CHO.CHO and HCHO distributions ~~are changing~~ then change from day to day. However, a large plume is ~~formed~~ clearly visible on ~~the 10th of~~ 10 August 2018. Enhanced CHO.CHO and HCHO columns are found at a distance of up to ~1500 km from the fires, indicating transport over long distances.

To investigate possible transport pathways, forward simulations of the atmospheric transport with FLEXPART were calculated for the ~~same period as HCHO and~~ of when CHO.CHO ~~observations~~ and HCHO plumes are observed (see Figure 4-B), assuming ~~a random~~ an effective lifetime of 14.4 hours. The latter is ~~in contrast to the~~ significantly longer than lifetimes of CHO.CHO and HCHO ~~expected, which are significantly shorter~~ found in the literature. On the other hand, the simulated pattern of air masses follows the ~~distribution of same distinctive path as~~ CHO.CHO and HCHO ~~columns well,~~

280 ~~showing VCDs. This shows good spatial agreement between simulations and satellite observations.~~ The tracer simulated with FLEXPART spreads over the same area as CHO.CHO, providing evidence for the transport of CHO.CHO and HCHO and their precursors over continental Canada. This is ~~even~~ more evident for the second period of interest in this study, which extends from the ~~20th~~20 to ~~21st~~21 of August 2018 (see Figure 7). While the spatial match of plume and model is good in this example, it is clear from the figure that ~~even~~ an effective lifetime of 14.4 hours does not describe fully the extent of ~~the trace gas transport, CHO.CHO~~ and ~~using HCHO transported. Using~~ shorter effective lifetimes for CHO.CHO and HCHO, taken form the literature would not reproduce the observations, ~~however. However~~ both lifetimes depend on time-of-day (daytime and nighttime) and also on photon flux conditions in the plume: on the diurnal photolysis and OH diurnal pattern cycles as well as on wet/dry deposition processes and other oxidants. Consequently, comparisons of FLEXPART simulations with different effective lifetimes were performed for two selected days, ~~which are detail discussed as is shown~~ in

285

290 Section 3.2.



295 **Figure 4. A) and B) Daily CHO.CHO and HCHO VCDs retrieved from S5P measurements for the period 7 to 10 of August 2018. C) Distribution of a tracer with a lifetime of 14.4 hours simulated with FLEXPART for the same period. The CHO.CHO in the plume decreases on average from 3×10^{15} molec.cm⁻² to 3×10^{14} molec.cm⁻², while the HCHO has a different variation in the plume but at the end of the plume, it decreases from 34×10^{16} molec.cm⁻² to 21×10^{16} molec.cm⁻². The FLEXPART tracer column decreases from 3×10^6 to 0.3×10^6 for this specific effective lifetime of 14.4 hours.**

3.2 Effective Lifetimes of CHO.CHO and HCHO in the plume

Figure 5 shows the results of FLEXPART simulations assuming effective lifetimes for a surrogate chemical species of ~2.9, 14.4, 23.1, and 28.9 hours for ~~the 10th~~10 and ~~20th~~20 of August 2018. From this figure, it is clear that only for the simulations having effective lifetimes of 23.1 hours or more, a significant fraction of the tracer emitted is present at the end

300

of the plume as observed in the measurements. This is ~~further~~also illustrated in Figure 6, depicting CHO.CHO and HCHO maps for ~~the 10th of 10~~10 August 2018. On top of these maps, contour lines are shown for the simulated air masses assuming effective lifetimes of ~2.9, 14.4, and 28.9 hours. It is evident that in both cases the tracer distributions simulated with longer effective lifetimes better describe the observed distribution of ~~glyoxal~~CHO.CHO and ~~formaldehyde~~HCHO.

305 Figures 7-A, -B, -C present a second comparison of daily maps of ~~glyoxal~~CHO.CHO and ~~formaldehyde~~HCHO VCDs with a FLEXPART tracer having ~~a~~an effective lifetime of 28.9 hours for ~~the period for 20th 20~~20 and ~~21st of 21~~21 August 2018. It is evident that again, the tracer follows the distribution of CHO.CHO and HCHO observations, similar to the first period studied (see Figure 4). However, on ~~20th 20~~20 and ~~21st of 21~~21 August 2018, the CHO.CHO ~~plume spreads~~and HCHO plumes spread over the ocean, where no ~~glyoxal or formaldehyde~~ sources are expected, ~~until it~~up to the point at which the plume disperses after being transported over a distance of about ~600 km ~~form~~from the fires.

310

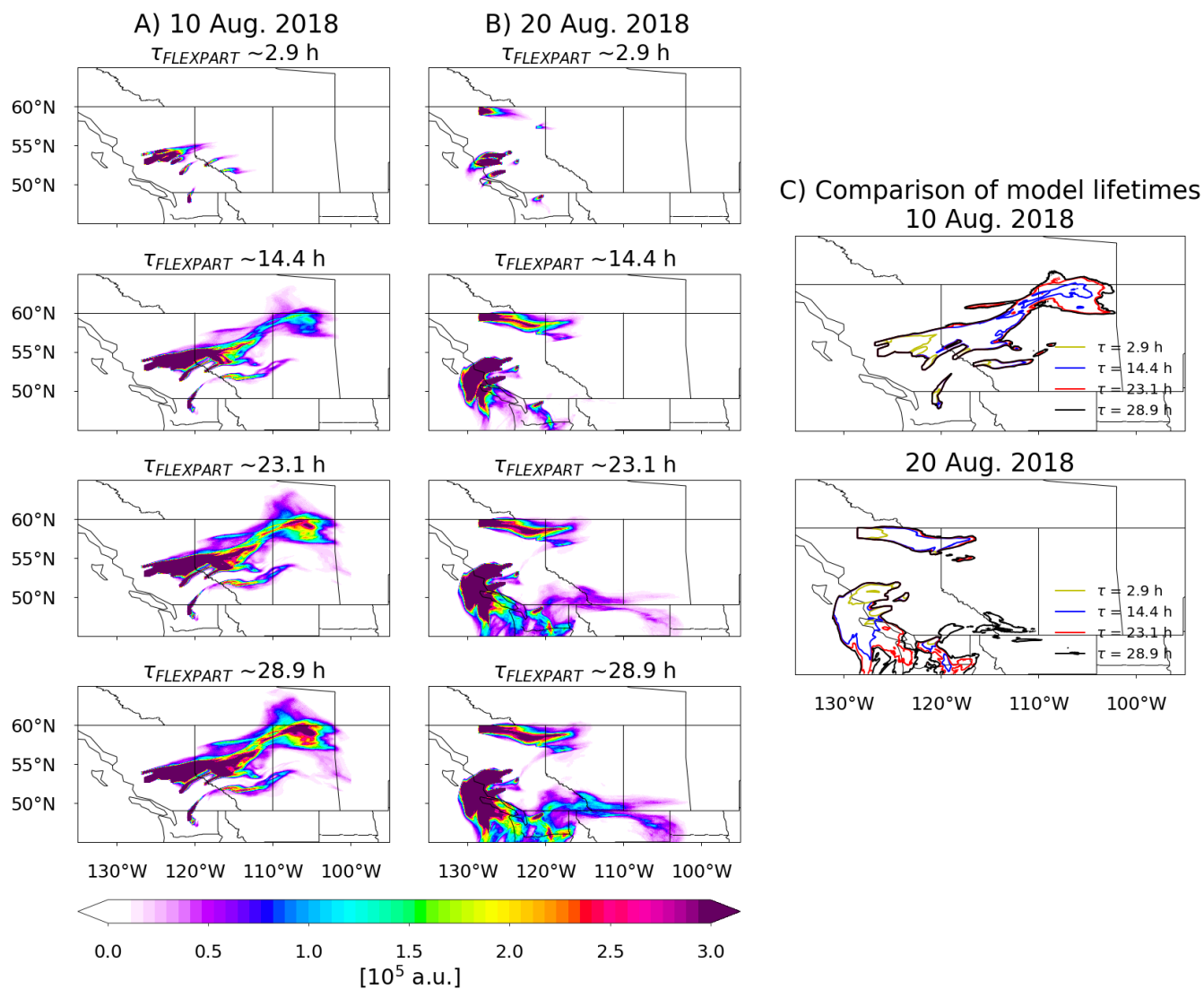


Figure 5. Daily maps of air masses simulated with FLEXPART for 10 and 20 ~~of~~ August 2018 are shown (A and B) for selected effective lifetimes (~2.9, 14.4, 23.1, 28.9 hours). C) Contour plots of simulations for the same lifetimes are compared for 10 and 20 ~~of~~ August 2018.

315 The observed behaviour of the CHO.CHO and HCHO plumes is in contrast with the short atmospheric lifetimes resulting from their rapid removal by photolysis and reaction with OH. In addition, CHO.CHO oligomerises and thus is a source of SOA formation (Schweitzer et al., 1998; Jang et al., 2002; Liggiio et al., 2005; Kroll et al., 2005; Loeffler et al., 2006; Volkamer et al., 2007; Fu et al., 2007; Myriokefalitakis et al., 2008; Stavrakou et al., 2009b, c). The simplest explanation of the observations of CHO.CHO and HCHO is that, during the fire events, both species are transported and/or produced during

320 transport, over long distances, resulting in an effective lifetime of about 28.9 hours. This would imply the transport of ~~the~~
VOC precursors of CHO.CHO and HCHO.

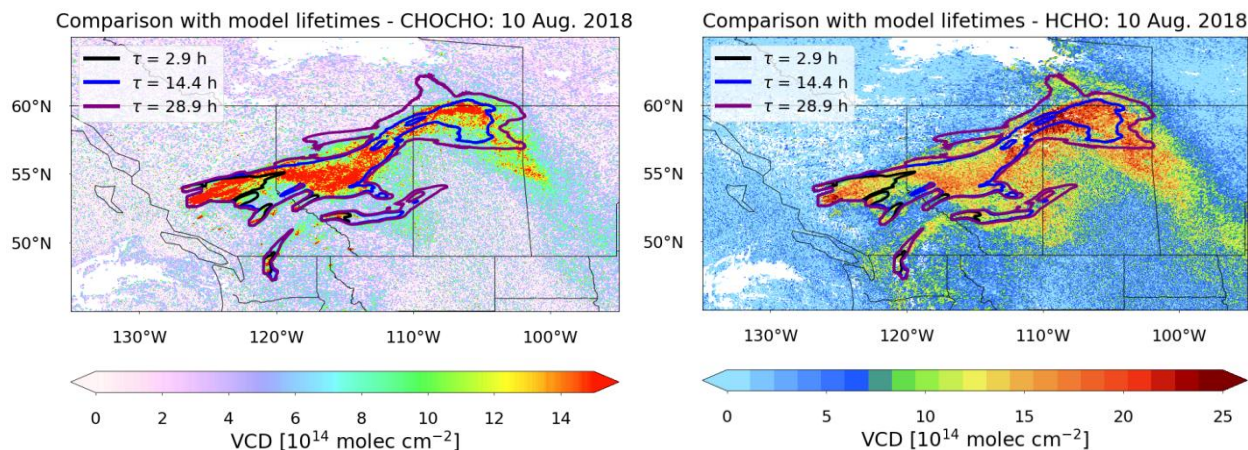


Figure 6. Daily maps CHO.CHO and HCHO VCD retrieved from S5P for 10th of August 2018 compared with FLEXPART tracer simulations having three different lifetimes (~2.9, 14.4, and 28.9 hours).

325 One reason for the ~~large dispersion~~ longer range transport of the CHO.CHO and HCHO plumes is the injection of the biomass burning emissions into the free troposphere, where high wind speeds favour transport over long distances. This is a well-known effect that has also been observed for NO₂ in GOME-2 data (Zien et al., 2014). However, even at high wind speeds, the short lifetime of these species would result in much smaller dispersed plumes than the ones observed. There are three possible explanations for this apparent contradiction:

330 Reason 1: The lifetimes of CHO.CHO and HCHO could be significantly longer than expected in these biomass burning plumes; if the OH mixing ratio and UV and visible radiation within the plume are much lower than outside the plume. There is, however, no indication that this should be the case; on the contrary, OH levels in the biomass burning plume are expected to be enhanced (~~Folkins et al., 1997~~), ~~leading to a reduction of the expected CHO.CHO lifetime in the unpolluted troposphere.~~ Folkins et al., 1997), leading to a reduction of the expected CHO.CHO and HCHO lifetimes. In this context, it
335 is interesting to investigate the NO₂ VCD observed. The NO₂ plumes coming from the biomass burning are shown in figure 8-B. During daytime NO₂ is removed in the gas phase by reaction with OH. Provided sufficient O₃ is present the photolysis of NO₂ produces NO and O which react respectively with O₃ to make NO₂ and oxygen molecules to make O₃. This is known as a “do nothing cycle”. NO₂ appears to decay relatively rapidly in the plumes coming from the fires. Our assumption that oxidation and photolysis of CHO.CHO and HCHO is relatively rapid, is thus not contradicted by the NO₂ decay in the fire
340 plumes.

Reason 2: There could be an efficient recycling process between the gas and aerosol phase, resulting in the observed extended effective lifetimes of CHO.CHO and HCHO. However, this reason is considered unlikely, because there is not yet any strong evidence of HCHO being a precursor of SOA formation, and as the shape of the plumes for both trace gases is similar, a similar mechanism is expected for both. Also, evidence for the release of CHO.CHO following the formation of oligomers in the aerosol phase, is limited (Kroll et al., 2005, and references therein).

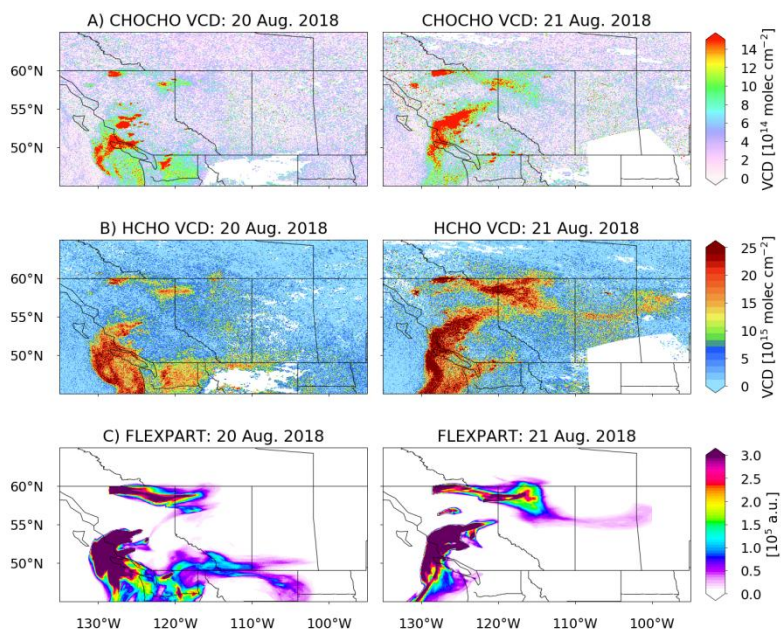


Figure 7. A) and B) Daily CHO.CHO and HCHO VCDs retrieved from S5P measurements for the period from 20 to 21 of August 2018. C) Tracer distribution simulated with FLEXPART for the same period assuming a lifetime of 28.9 hours. Enhanced CHO.CHO columns spread over the ocean in a pattern similar to that simulated by the model tracer.

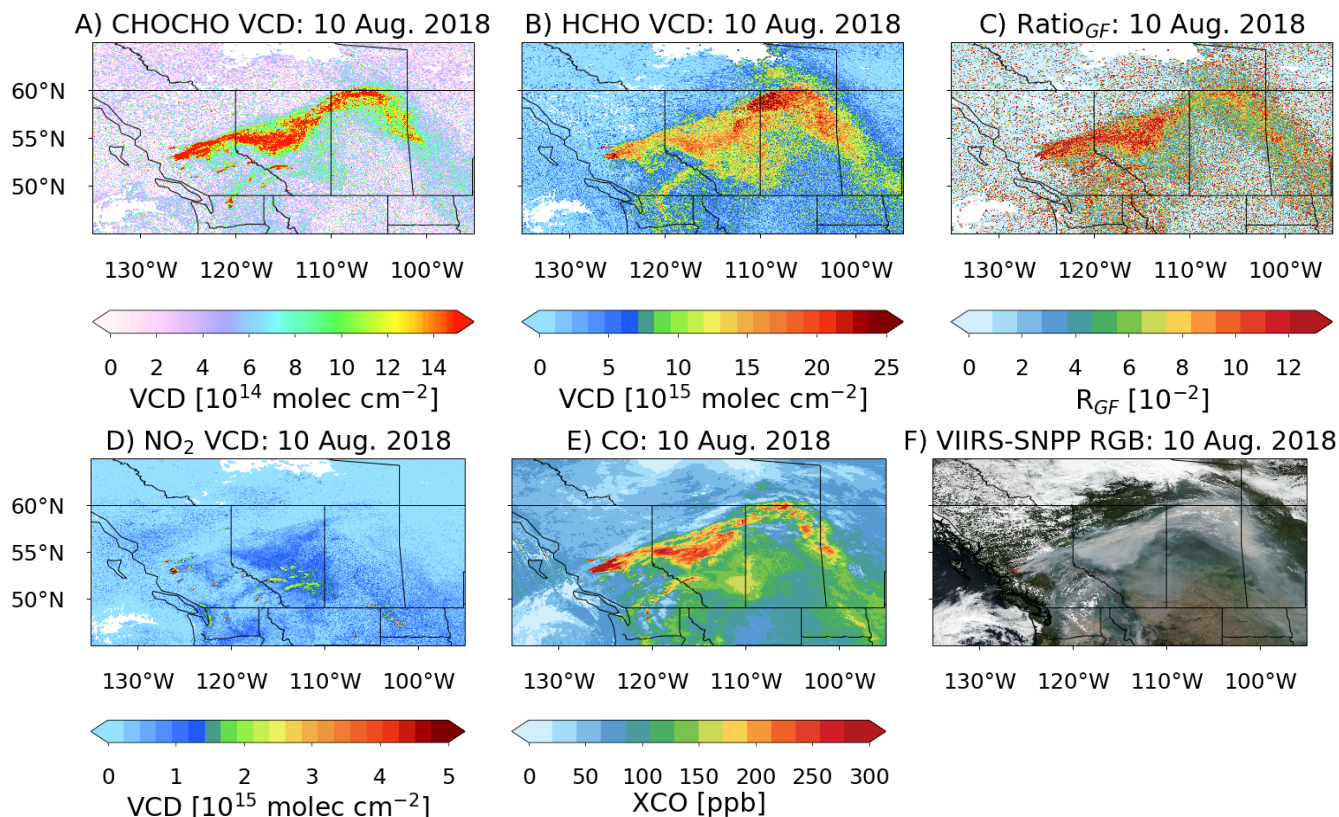
Reason 3: The plume could contain glyoxal-CHO.CHO and formaldehyde-HCHO precursors, i.e. VOCs, which are slowly produce additional VOCs-oxidized, releasing CHO.CHO and HCHO along the trajectory, resulting. If true, this would result in an apparent increase in lifetime. In order to better assess the CHO.CHO and HCHO spatial distribution seen on the 10th of 10 August 2018, two additional S5P-TROPOMI retrievals have been taken into account; the column-averaged dry air mole fractions of CO, retrieved by the algorithm described in Schneising et al. (2019), and the VCD NO₂ VCD retrieved using an algorithm similar to the one described for the GOME-2 instrument (Richter et al., 2011) and using AMF calculated following the same approach as the one described before for glyoxal-CHO.CHO and formaldehyde-HCHO (see section 2.3). The CO plume shows a similar spatial behavior as HCHO-pattern to those of CHO.CHO and CHO.CHO-HCHO (see Figure 8-E)-8-E). As CO is a relatively long-lived tracer of fire emissions, having a lifetime with respect to OH of months, this is further confirmation for the fact that supports the fire origin of the VOCs and/or their precursors originate from the fires and then undergo long range transport. plume. As noted above, NO₂ is removed by OH faster than CHO.CHO and HCHO. The NO₂

VCD enhancements, in contrast ~~to those of CHO.CHO and HCHO~~, are limited to the proximity of the fire hot-spots (see Figure 8-D). This ~~is the~~ behaviour ~~ur expected~~ agrees with that assumed for a molecule with a short atmospheric lifetime ~~and highlights how unusual the behavior of the VOCs is.~~ A true-colour image from the Visible Infrared Imaging Radiometer Suite (VIIRS) clearly shows the distribution of smoke and aerosols produced because of the emission from the fires being transported and transformed (Figure 8-F). The distribution of the aerosol appears qualitatively to be similar to the CHO.CHO, HCHO, and CO distributions, ~~indicating. We infer that these species~~ the transported plumes are mixed in the aerosol layer mixtures of CO, CHO.CHO, HCHO, aerosol and presumably other pollutants released by the fire. It is interesting to note that CHO.CHO and CO follow mainly the main plume, while the HCHO distribution is more ~~diffused~~ diffuse and shows enhanced values also over regions where a thinner aerosol plume is visible in the VIIRS image. ~~This may possibly originating~~ originate from ~~another unidentified fires as this part of the plume~~ or another unknown source, which is not ~~apparent~~ included in ~~the our~~ FLEXPART simulations.

As ~~an~~ additional criterion ~~information~~, the ratio of CHO.CHO glyoxal to HCHO formaldehyde (R_{GF}) is ~~shown~~ presented in Figure 8-C. Larger values of R_{GF} are found close to the location of the wildfires as already reported in previous publications (Vrekoussis et al., 2010). This is an indication of enhanced primary emissions of glyoxal CHO.CHO relative to those of HCHO from fires. ~~Progressively lower~~ Lower R_{GF} values are ~~then~~ found ~~until~~ closer to the end of the plume ~~suggesting either a implying a~~ decreasing of glyoxal production over time or a change of CHO.CHO relative to that for of HCHO during the transport of polluted air in the fire emissions injected into the plume. Another potential explanation would be the mixing in of air from different origins, having lower CHO.CHO and/or higher HCHO different concentrations of the trace gases, during the plume transport. This is however not confirmed by the observed CO behaviour, which shows a similar spatial distribution to CHO.CHO and HCHO.

The comparison of retrieved S5P columns and FLEXPART tracer simulations discussed is based on a number of simplifications. ~~First of all, the~~ The observational conditions of the biomass burning plumes are complex, and aerosol scattering and absorption ~~certainly~~ impact on the sensitivity of the retrievals. While this is taken into account by using air mass factors for elevated plumes positioned at altitudes derived from CALIPSO observations, there ~~is~~ remains considerable uncertainty with respect to absolute values. Aerosol loading and optical properties will vary ~~over~~ along the plume and thus ~~will~~ the retrieval sensitivities, ~~and this is.~~ This not modelled ~~here explicitly in this study.~~ However, the differences apparent between the spatial distributions of glyoxal CHO.CHO and NO_2 , which are retrieved in ~~very~~ similar spectral regions, provide evidence for the fact that measurement sensitivity ~~is~~ does not ~~explain~~ the driver for differences in the observed VCD plume patterns. Another crucial simplification is the assumption of a constant fire emissions and the proportionality of FRP and emission strength in the FLEXPART simulations. In reality, fire emissions will also depend on the type of biomass burned, the age of the fire, the time of the day and the environmental conditions, and this will have an effect on the trace gas distribution along the plume, which reflects both chemical transformation and the history of emissions. Modelling of this

time-evolution is complex, if possible at all, and out of the scope of this study. However, the observation that both CHO.CHO and HCHO are present in the biomass burning plume after extended time periods and over long distances is robust and ~~can only be~~ best explained by ~~continuous~~ the release of CHO.CHO and HCHO from the transformation of longer-lived precursors and/or efficient recycling processes in the plume as discussed above.



400 | **Figure 8.** Panels A, B, D, and E show the CHO.CHO, HCHO, NO₂, and CO columns, respectively retrieved from S5P measurements for 10th of August 2018. Note that CO columns are unfiltered and only represent a qualitative description of the plume. The AMFs used for CHO.CHO, HCHO, and NO₂ are appropriate for the biomass burning plume only. Panel C depicts the calculated CHO.CHO ~~to~~ HCHO (R_{GF}) for the same day. Panel F shows a true color ur image of the aerosol distribution from VIIRS for 10th of August 2018.

4 Summary and ~~conlusions~~ conclusions

405 | The retrieval of ~~formaldehyde and glyoxal total column amounts~~ CHO.CHO and HCHO VCDs from measurements of the TROPOMI instrument on board the Sentinel-5P satellite is reported. This ~~enables the extension of~~ will extend ~~the datasets~~ already available from the SCIAMACHY, GOME-2, and OMI instruments, ~~and shows the~~ The advantage of the high spatial

resolution and low noise of TROPOMI for studying specific geophysical phenomena. ~~The is well demonstrated in the features and plumes seen in the CHO.CHO, HCHO, CO, and NO₂ VCDs.~~

410 In this case study the satellite data show clear evidence for pyrogenic emissions of CHO.CHO and HCHO ~~and their precursors~~ during the wildfire season in summer 2018 in British Columbia, Canada. The spatial and temporal pattern of the highest retrieved CHO.CHO and HCHO ~~columns~~VCDs are associated with areas having high fire radiative power, as ~~observed-identified~~ in the MODIS fire data products, ~~indicating~~. This indicates that in these areas, pyrogenic emissions are the dominant ~~sources~~source of CHO.CHO and HCHO. In addition to local enhancements of NO₂, CHO.CHO, and HCHO, ~~an~~close to the fires, extended ~~plume~~plumes of elevated CHO.CHO and HCHO ~~amounts is~~VCD are observed ~~on some days~~ downwind ~~of the fires~~. ~~This finding provides evidence of either a) long range transported VOCs, primarily emitted from the fires or b) their production from precursor species during the transport of.~~ This is in contrast with the plume-behaviour of NO₂, which is also transported but is short lived. ~~The spatial and temporal~~ VOCCHO.CHO and HCHO distribution observed from satellite follows ~~the same~~a similar pattern ~~asto~~ that of CO₂, which is long lived, and that simulated by the ~~FLEXPART~~ dispersion model, initialized by tracer emissions starting at known fire locations. Enhanced CHO.CHO and HCHO ~~columns~~ were found in the S5P data up to 1500 km from their sources.

In order to obtain reasonable agreement between the model results and the measurements, an effective tracer lifetime of more than 20 hours and up to 28.9 hours needs to be assumed in the FLEXPART simulations. This is significantly longer than the anticipated lifetimes of glyoxalCHO.CHO and formaldehydeHCHO. The ~~long~~ transport of glyoxalCHO.CHO and ~~formaldehyde in~~HCHO along the length of the plume could be associated with ~~the lifting of glyoxal and formaldehyde~~these traces gases being lifted from the boundary layer into the free troposphere, where high wind speeds lead to rapid transport. The long apparent lifetime of CHO.CHO and HCHO in the transported plumes could ~~either~~ be explained by a real increase in ~~atmospheric~~their lifetime due toin the specific-plume because of photochemical conditions in the biomass-burning-plume ~~or as we attribute, the presence of longer lived precursors~~plume, which ~~are oxidized to form CHO.CHO and HCHO during transport.~~we consider unexpected. Based on our current knowledge, the most probable explanation of the apparent long lifetime of CHO.CHO and HCHO would be ~~the latter where~~ formation ~~of glyoxal and formaldehyde~~ within the plume is caused by the oxidation of a mixture of longer-lived emitted VOC speciesprecursors (e.g. methanol, ethanol, acetylene, aromatics, glycolaldehyde, ethylene etc.), that ~~in turn,~~ form CHO.CHO and HCHO ~~at~~ different rates. Further research is needed to investigate how frequent such fire-related long-~~range~~ transport events of VOCs are, ~~what the exact.~~ The chemical mechanism of the formation ~~within the plume is and how~~of the CHO.CHO and HCHO in the plumes downwind of the fires needs to be identified. The assessment of the number of such fires events ~~impact on ozone~~and their relevance for tropospheric O₃ and aerosol production downwind of the fires and air quality ~~downwind of the fires~~is required.

440 | *Author contributions.* L. M. A. Alvarado, A. Richter and J. P. Burrows have prepared the manuscript with the contribution of
all authors and developed the glyoxal and formaldehyde and NO₂ retrievals for TROPOMI measurements. M. Vrekoussis, A.
Hilboll and A. B. Kalisz Hedegaard have designed and performed the FLEXPART ~~experiment for simulation~~ [simulations](#) of
the airmass~~ess~~ assuming different effective lifetimes. O. Schneising has developed the CO retrieval and provided the CO
data for the comparison with glyoxal and formaldehyde products.

445 | *Acknowledgements.* The authors acknowledge financial support provided by the University of Bremen. Copernicus Sentinel-
5P lv1 data from 2018 were used in this study. This publication contains modified COPERNICUS Sentinel data (2018). We
thank the MACC team for providing the GFASv1.0 FRP and injection height products. FLEXPART simulations were
conducted on the University of Bremen's HPC cluster Aether, funded by DFG [within the scope of the Excellence Initiative](#).
VIIRS and CALIPSO data were obtained from the NASA Langley Research Center Atmospheric Science Data Center.
450 | [FLEXPART simulation results were generated using Copernicus Climate Change Service Information \(ERA5\)](#).

This is in part preparatory work for the analysis of the data from the DFG SPP HALO EMeRGe project, [which has one focus
on biomass burning and the long range transport of such plumes. We thank Abram Sanders \(European Organisation for the
Exploitation of Meteorological Satellites, Darmstadt\) for providing support in the preparation of CALIPSO data for the
computation of CHO,CHO and HCHO AMFs.](#)

455 | **References**

- Abbot, D. S., Palmer, P. I., Martin, R. V., Chance, K. V., Jacob, D. J. and Guenther, A.: Seasonal and interannual variability
of North American isoprene emissions as determined by formaldehyde column measurements from space, *Geophysical
Research Letters*, 30(17), doi:10.1029/2003GL017336, 2003.
- 460 | Alvarado, L. M. A.: Investigating the role of glyoxal using satellite and MAX-DOAS measurements, PhD, University of
Bremen., 2016.
- Alvarado, L. M. A., Richter, A., Vrekoussis, M., Wittrock, F., Hilboll, A., Schreier, S. F. and Burrows, J. P.: An improved
glyoxal retrieval from OMI measurements, *Atmos. Meas. Tech.*, 7(12), 4133–4150, doi:10.5194/amt-7-4133-2014, 2014.

465

- Alvarado, L. M. A., Richter, A., Vrekoussis, M., Wittrock, F., Hilboll, A., Schreier, S. F. and Burrows, J. P.: Investigating the Link Between Glyoxal and Biogenic Activities, in *Towards an Interdisciplinary Approach in Earth System Science*, edited by G. Lohmann, H. Meggers, V. Unnithan, D. Wolf-Gladrow, J. Notholt, and A. Bracher, pp. 59–65, Springer International Publishing., 2015.
- 470 Atkinson, R.: Atmospheric chemistry of VOCs and NO_x, *Atmospheric Environment*, 34(12–14), 2063–2101, doi:10.1016/S1352-2310(99)00460-4, 2000.
- Behrens, L. K., Hilboll, A., Richter, A., Peters, E., Alvarado, L. M. A., Kalisz Hedegaard, A. B., Wittrock, F., Burrows, J. P. and Vrekoussis, M.: Detection of outflow of formaldehyde and glyoxal from the African continent to the Atlantic Ocean with a MAX-DOAS instrument, *Atmospheric Chemistry and Physics*, 19(15), 10257–10278, doi:<https://doi.org/10.5194/acp-19-10257-2019>, 2019.
- 480 Bovensmann, H., Burrows, J. P., Buchwitz, M., Frerick, J., Noël, S., Rozanov, V. V., Chance, K. V. and Goede, A. P. H.: SCIAMACHY: Mission Objectives and Measurement Modes, *Journal of the Atmospheric Sciences*, 56(2), 127–150, doi:10.1175/1520-0469(1999)056<0127:SMOAMM>2.0.CO;2, 1999.
- Burrows, J. P., Hölzle, E., Goede, A. P. H., Visser, H. and Fricke, W.: SCIAMACHY—scanning imaging absorption spectrometer for atmospheric cartography, *Acta Astronautica*, 35(7), 445–451, doi:10.1016/0094-5765(94)00278-T, 1995.
- 485 Burrows, J. P., Weber, M., Buchwitz, M., Rozanov, V., Ladstätter-Weissenmayer, A., Richter, A., DeBeek, R., Hoogen, R., Bramstedt, K., Eichmann, K.-U., Eisinger, M. and Perner, D.: The Global Ozone Monitoring Experiment (GOME): Mission Concept and First Scientific Results, *Journal of the Atmospheric Sciences*, 56(2), 151–175, doi:10.1175/1520-0469(1999)056<0151:TGOMEG>2.0.CO;2, 1999.
- 490 Chan Miller, C., Gonzalez Abad, G., Wang, H., Liu, X., Kurosu, T., Jacob, D. J. and Chance, K.: Glyoxal retrieval from the Ozone Monitoring Instrument, *Atmos. Meas. Tech.*, 7(11), 3891–3907, doi:10.5194/amt-7-3891-2014, 2014.

De Smedt, I., Müller, J.-F., Stavrakou, T., van der A, R., Eskes, H. and Van Roozendael, M.: Twelve years of global observations of formaldehyde in the troposphere using GOME and SCIAMACHY sensors, *Atmos. Chem. Phys.*, 8(16), 4947–4963, doi:10.5194/acp-8-4947-2008, 2008.

500

De Smedt, I., Van Roozendael, M., Stavrakou, T., Müller, J.-F., Lerot, C., Theys, N., Valks, P., Hao, N. and van der A, R.: Improved retrieval of global tropospheric formaldehyde columns from GOME-2/MetOp-A addressing noise reduction and instrumental degradation issues, *Atmos. Meas. Tech.*, 5(11), 2933–2949, doi:10.5194/amt-5-2933-2012, 2012.

De Smedt, I., Stavrakou, T., Hendrick, F., Danckaert, T., Vlemmix, T., Pinardi, G., Theys, N., Lerot, C., Gielen, C., Vigouroux, C., Hermans, C., Fayt, C., Veefkind, P., Müller, J.-F. and Van Roozendael, M.: Diurnal, seasonal and long-term variations of global formaldehyde columns inferred from combined OMI and GOME-2 observations, *Atmos. Chem. Phys.*, 15(21), 12519–12545, doi:10.5194/acp-15-12519-2015, 2015.

505

De Smedt, I., Theys, N., Yu, H., Danckaert, T., Lerot, C., Compernelle, S., Roozendael, M. V., Richter, A., Hilboll, A., Peters, E., Pedernana, M., Loyola, D., Beirle, S., Wagner, T., Eskes, H., Geffen, J. van, Boersma, K. F. and Veefkind, P.: Algorithm theoretical baseline for formaldehyde retrievals from S5P TROPOMI and from the QA4ECV project, *Atmospheric Measurement Techniques*, 11(4), 2395–2426, doi:https://doi.org/10.5194/amt-11-2395-2018, 2018.

510

Fleischmann, O. C., Hartmann, M., Burrows, J. P. and Orphal, J.: New ultraviolet absorption cross-sections of BrO at atmospheric temperatures measured by time-windowing Fourier transform spectroscopy, *Journal of Photochemistry and Photobiology A: Chemistry*, 168(1–2), 117–132, doi:10.1016/j.jphotochem.2004.03.026, 2004.

515 Folkins, I., Wennberg, P. O., Hanisco, T. F., Anderson, J. G. and Salawitch, R. J.: OH, HO₂, and NO in two biomass burning plumes: Sources of HO_x and implications for ozone production, *Geophysical Research Letters*, 24(24), 3185–3188, doi:10.1029/97GL03047, 1997.

Fu, T.-M., Jacob, D. J., Palmer, P. I., Chance, K., Wang, Y. X., Barletta, B., Blake, D. R., Stanton, J. C. and Pilling, M. J.:
520 Space-based formaldehyde measurements as constraints on volatile organic compound emissions in east and south Asia and
implications for ozone, *Journal of Geophysical Research: Atmospheres*, 112(D6), n/a–n/a, doi:10.1029/2006JD007853,
2007.

González Abad, G., Liu, X., Chance, K., Wang, H., Kurosu, T. P. and Suleiman, R.: Updated Smithsonian Astrophysical
525 Observatory Ozone Monitoring Instrument (SAO OMI) formaldehyde retrieval, *Atmos. Meas. Tech.*, 8(1), 19–32,
doi:10.5194/amt-8-19-2015, 2015.

Guenther, A., Geron, C., Pierce, T., Lamb, B., Harley, P. and Fall, R.: Natural emissions of non-methane volatile organic
compounds, carbon monoxide, and oxides of nitrogen from North America, *Atmospheric Environment*, 34(12–14), 2205–
530 2230, doi:10.1016/S1352-2310(99)00465-3, 2000.

Guenther, A., Karl, T., Harley, P., Wiedinmyer, C., Palmer, P. I. and Geron, C.: Estimates of global terrestrial isoprene
emissions using MEGAN (Model of Emissions of Gases and Aerosols from Nature), *Atmos. Chem. Phys.*, 6(11), 3181–
3210, doi:10.5194/acp-6-3181-2006, 2006.

535

Hewson, W., Bösch, H., Barkley, M. P. and De Smedt, I.: Characterisation of GOME-2 formaldehyde retrieval sensitivity,
Atmos. Meas. Tech., 6(2), 371–386, doi:10.5194/amt-6-371-2013, 2013.

Jang, M., Czoschke, N. M., Lee, S. and Kamens, R. M.: Heterogeneous Atmospheric Aerosol Production by Acid-Catalyzed
540 Particle-Phase Reactions, *Science*, 298(5594), 814–817, doi:10.1126/science.1075798, 2002.

Justice, C. O., Giglio, L., Korontzi, S., Owens, J., Morisette, J. T., Roy, D., Descloitres, J., Alleaume, S., Petitcolin, F. and

Kaufman, Y.: The MODIS fire products, *Remote Sensing of Environment*, 83(1–2), 244–262, doi:10.1016/S0034-4257(02)00076-7, 2002.

545

Kaiser, J. W., Heil, A., Andreae, M. O., Benedetti, A., Chubarova, N., Jones, L., Morcrette, J.-J., Razinger, M., Schultz, M. G., Suttie, M. and van der Werf, G. R.: Biomass burning emissions estimated with a global fire assimilation system based on observed fire radiative power, *Biogeosciences*, 9(1), 527–554, doi:10.5194/bg-9-527-2012, 2012.

550 Kansal, A.: Sources and reactivity of NMHCs and VOCs in the atmosphere: A review, *Journal of Hazardous Materials*, 166(1), 17–26, doi:10.1016/j.jhazmat.2008.11.048, 2009.

Kroll, J. H., Ng, N. L., Murphy, S. M., Varutbangkul, V., Flagan, R. C. and Seinfeld, J. H.: Chamber studies of secondary organic aerosol growth by reactive uptake of simple carbonyl compounds, *J. Geophys. Res.*, 110(D23), D23207, doi:10.1029/2005JD006004, 2005.

Kurosu, T. P., Chance, K. and Volkamer, R.: Measurements of HCHO, CHOCHO, and BrO from the Ozone Monitoring Instrument on EOS AURA, in *Proceedings of Envisat Symposium.*, 2007.

560 Lerot, C., Stavrou, T., De Smedt, I., Müller, J.-F. and Van Roozendaal, M.: Glyoxal vertical columns from GOME-2 backscattered light measurements and comparisons with a global model, *Atmos. Chem. Phys.*, 10(24), 12059–12072, doi:10.5194/acp-10-12059-2010, 2010.

Levelt, P. F., van den Oord, G. H. J., Dobber, M. R., Malkki, A., Visser, H., Vries, J. de, Stammes, P., Lundell, J. O. V. and Saari, H.: The ozone monitoring instrument, *IEEE Transactions on Geoscience and Remote Sensing*, 44(5), 1093 – 1101, doi:10.1109/TGRS.2006.872333, 2006.

Liggio, J., Li, S.-M. and McLaren, R.: Reactive uptake of glyoxal by particulate matter, *Journal of Geophysical Research: Atmospheres*, 110(D10), doi:10.1029/2004JD005113, 2005.

570

Liu, Z., Wang, Y., Vrekoussis, M., Richter, A., Wittrock, F., Burrows, J. P., Shao, M., Chang, C.-C., Liu, S.-C., Wang, H. and Chen, C.: Exploring the missing source of glyoxal (CHOCHO) over China, *Geophysical Research Letters*, 39(10), doi:10.1029/2012GL051645, 2012.

575 Loeffler, K. W., Koehler, C. A., Paul, N. M. and De Haan, D. O.: Oligomer Formation in Evaporating Aqueous Glyoxal and Methyl Glyoxal Solutions, *Environ. Sci. Technol.*, 40(20), 6318–6323, doi:10.1021/es060810w, 2006.

580 Marais, E. A., Jacob, D. J., Kurosu, T. P., Chance, K., Murphy, J. G., Reeves, C., Mills, G., Casadio, S., Millet, D. B., Barkley, M. P., Paulot, F. and Mao, J.: Isoprene emissions in Africa inferred from OMI observations of formaldehyde columns, *Atmos. Chem. Phys.*, 12(14), 6219–6235, doi:10.5194/acp-12-6219-2012, 2012.

Mason, J. D., Cone, M. T. and Fry, E. S.: Ultraviolet (250–550 nm) absorption spectrum of pure water, *Appl. Opt.*, AO, 55(25), 7163–7172, doi:10.1364/AO.55.007163, 2016.

585 Meller, R. and Moortgat, G. K.: Temperature dependence of the absorption cross sections of formaldehyde between 223 and 323 K in the wavelength range 225–375 nm, *J. Geophys. Res.*, 105(D6), 7089–7101, doi:10.1029/1999JD901074, 2000.

590 Munro, R., Lang, R., Klaes, D., Poli, G., Retscher, C., Lindstrot, R., Huckle, R., Lacan, A., Grzegorski, M., Holdak, A., Kokhanovsky, A., Livschitz, J. and Eisinger, M.: The GOME-2 instrument on the Metop series of satellites: instrument design, calibration, and level 1 data processing – an overview, *Atmos. Meas. Tech.*, 9(3), 1279–1301, doi:10.5194/amt-9-1279-2016, 2016.

Myriokefalitakis, S., Vrekoussis, M., Tsigaridis, K., Wittrock, F., Richter, A., Brühl, C., Volkamer, R., Burrows, J. P. and Kanakidou, M.: The influence of natural and anthropogenic secondary sources on the glyoxal global distribution, *Atmos. Chem. Phys.*, 8(16), 4965–4981, doi:10.5194/acp-8-4965-2008, 2008.

Natural Resources Canada: Canadian Wildland Fire Information System | Archived reports, [online] Available from: <http://cwfis.cfs.nrcan.gc.ca/report/archives?year=2018&month=08&day=29&process=Submit> (Accessed 12 April 2019), 2018.

600

Palmer, P. I., Jacob, D. J., Chance, K., Martin, R. V., Spurr, R. J. D., Kurosu, T. P., Bey, I., Yantosca, R., Fiore, A. and Li, Q.: Air mass factor formulation for spectroscopic measurements from satellites: Application to formaldehyde retrievals from the Global Ozone Monitoring Experiment, *Journal of Geophysical Research: Atmospheres*, 106(D13), 14539–14550, doi:10.1029/2000JD900772, 2001.

605

Palmer, P. I., Jacob, D. J., Fiore, A. M., Martin, R. V., Chance, K. and Kurosu, T. P.: Mapping isoprene emissions over North America using formaldehyde column observations from space, *Journal of Geophysical Research: Atmospheres*, 108(D6), n/a–n/a, doi:10.1029/2002JD002153, 2003.

610 Pisso, I., Sollum, E., Grythe, H., Kristiansen, N., Cassiani, M., Eckhardt, S., Arnold, D., Morton, D., Thompson, R. L., Groot Zwaaftink, C. D., Evangeliou, N., Sodemann, H., Haimberger, L., Henne, S., Brunner, D., Burkhart, J. F., Fouilloux, A., Brioude, J., Philipp, A., Seibert, P. and Stohl, A.: The Lagrangian particle dispersion model FLEXPART version 10.3, *Geoscientific Model Development Discussions*, 1–67, doi:https://doi.org/10.5194/gmd-2018-333, 2019.

615 Puķīte, J., Kühn, S., Deutschmann, T., Platt, U. and Wagner, T.: Extending differential optical absorption spectroscopy for limb measurements in the UV, *Atmos. Meas. Tech.*, 3(3), 631–653, doi:10.5194/amt-3-631-2010, 2010.

Rémy, S., Veira, A., Paugam, R., Sofiev, M., Kaiser, J. W., Marengo, F., Burton, S. P., Benedetti, A., Engelen, R. J., Ferrare, R. and Hair, J. W.: Two global data sets of daily fire emission injection heights since 2003, *Atmospheric Chemistry and Physics*, 17(4), 2921–2942, doi:<https://doi.org/10.5194/acp-17-2921-2017>, 2017.

Richter, A., Begoin, M., Hilboll, A. and Burrows, J. P.: An improved NO₂ retrieval for the GOME-2 satellite instrument, *Atmos. Meas. Tech.*, 4(6), 1147–1159, doi:[10.5194/amt-4-1147-2011](https://doi.org/10.5194/amt-4-1147-2011), 2011.

625 Rothman, L. S., Gordon, I. E., Babikov, Y., Barbe, A., Chris Benner, D., Bernath, P. F., Birk, M., Bizzocchi, L., Boudon, V., Brown, L. R., Campargue, A., Chance, K., Cohen, E. A., Coudert, L. H., Devi, V. M., Drouin, B. J., Fayt, A., Flaud, J.-M., Gamache, R. R., Harrison, J. J., Hartmann, J.-M., Hill, C., Hodges, J. T., Jacquemart, D., Jolly, A., Lamouroux, J., Le Roy, R. J., Li, G., Long, D. A., Lyulin, O. M., Mackie, C. J., Massie, S. T., Mikhailenko, S., Müller, H. S. P., Naumenko, O. V., Nikitin, A. V., Orphal, J., Perevalov, V., Perrin, A., Polovtseva, E. R., Richard, C., Smith, M. A. H., Starikova, E., Sung, K.,
630 Tashkun, S., Tennyson, J., Toon, G. C., Tyuterev, V. G. and Wagner, G.: The HITRAN2012 molecular spectroscopic database, *Journal of Quantitative Spectroscopy and Radiative Transfer*, 130, 4–50, doi:[10.1016/j.jqsrt.2013.07.002](https://doi.org/10.1016/j.jqsrt.2013.07.002), 2013.

Rozanov, V. V., Rozanov, A. V., Kokhanovsky, A. A. and Burrows, J. P.: Radiative transfer through terrestrial atmosphere and ocean: Software package SCIATRAN, *Journal of Quantitative Spectroscopy and Radiative Transfer*,
635 doi:[10.1016/j.jqsrt.2013.07.004](https://doi.org/10.1016/j.jqsrt.2013.07.004), 2013.

Schneising, O., Buchwitz, M., Reuter, M., Bovensmann, H., Burrows, J. P., Borsdorff, T., Deutscher, N. M., Feist, D. G., Griffith, D. W. T., Hase, F., Hermans, C., Iraci, L. T., Kivi, R., Landgraf, J., Morino, I., Notholt, J., Petri, C., Pollard, D. F., Roche, S., Shiomi, K., Strong, K., Sussmann, R., Velasco, V. A., Warneke, T. and Wunch, D.: A scientific algorithm to
640 simultaneously retrieve carbon monoxide and methane from TROPOMI onboard Sentinel-5 Precursor, *Atmospheric Measurement Techniques Discussions*, 1–44, doi:<https://doi.org/10.5194/amt-2019-243>, 2019.

Schweitzer, F., Magi, L., Mirabel, P. and George, C.: Uptake Rate Measurements of Methanesulfonic Acid and Glyoxal by Aqueous Droplets, *J. Phys. Chem. A*, 102(3), 593–600, doi:[10.1021/jp972451k](https://doi.org/10.1021/jp972451k), 1998.

Serdyuchenko, A., Gorshelev, V., Weber, M., Chehade, W. and Burrows, J. P.: High spectral resolution ozone absorption cross-sections – Part 2: Temperature dependence, *Atmospheric Measurement Techniques*, 7(2), 625–636, doi:<https://doi.org/10.5194/amt-7-625-2014>, 2014.

650 Sinreich, R., Volkamer, R., Filsinger, F., Frieß, U., Kern, C., Platt, U., Sebastián, O. and Wagner, T.: MAX-DOAS detection of glyoxal during ICARTT 2004, *Atmos. Chem. Phys.*, 7(5), 1293–1303, doi:10.5194/acp-7-1293-2007, 2007.

Sinreich, R., Coburn, S., Dix, B. and Volkamer, R.: Ship-based detection of glyoxal over the remote tropical Pacific Ocean, *Atmos. Chem. Phys.*, 10(23), 11359–11371, doi:10.5194/acp-10-11359-2010, 2010.

Stavrakou, T., Müller, J.-F., De Smedt, I., Van Roozendael, M., van der Werf, G. R., Giglio, L. and Guenther, A.: Evaluating the performance of pyrogenic and biogenic emission inventories against one decade of space-based formaldehyde columns, *Atmos. Chem. Phys.*, 9(3), 1037–1060, doi:10.5194/acp-9-1037-2009, 2009a.

660 Stavrakou, T., Müller, J.-F., De Smedt, I., Van Roozendael, M., van der Werf, G. R., Giglio, L. and Guenther, A.: Global emissions of non-methane hydrocarbons deduced from SCIAMACHY formaldehyde columns through 2003–2006, *Atmos. Chem. Phys.*, 9(11), 3663–3679, doi:10.5194/acp-9-3663-2009, 2009b.

665 Stavrakou, T., Müller, J.-F., De Smedt, I., Van Roozendael, M., Kanakidou, M., Vrekoussis, M., Wittrock, F., Richter, A. and Burrows, J. P.: The continental source of glyoxal estimated by the synergistic use of spaceborne measurements and inverse modelling, *Atmos. Chem. Phys.*, 9(21), 8431–8446, doi:10.5194/acp-9-8431-2009, 2009c.

Stohl, A., Forster, C., Frank, A., Seibert, P. and Wotawa, G.: Technical note: The Lagrangian particle dispersion model FLEXPART version 6.2, *Atmospheric Chemistry and Physics*, 5(9), 2461–2474, doi:<https://doi.org/10.5194/acp-5-2461-2005>, 2005.

Thalman, R., Baeza-Romero, M. T., Ball, S. M., Borrás, E., Daniels, M. J. S., Goodall, I. C. A., Henry, S. B., Karl, T., Keutsch, F. N., Kim, S., Mak, J., Monks, P. S., Muñoz, A., Orlando, J., Peppe, S., Rickard, A. R., Ródenas, M., Sánchez, P., Seco, R., Su, L., Tyndall, G., Vázquez, M., Vera, T., Waxman, E. and Volkamer, R.: Instrument intercomparison of glyoxal, methyl glyoxal and NO₂ under simulated atmospheric conditions, *Atmos. Meas. Tech.*, 8(4), 1835–1862, doi:10.5194/amt-8-1835-2015, 2015.

Urbanski, S. P., Reeves, M. C., Corley, R. E., Silverstein, R. P. and Hao, W. M.: Contiguous United States wildland fire emission estimates during 2003–2015, *Earth System Science Data*, 10(4), 2241–2274, doi:<https://doi.org/10.5194/essd-10-2241-2018>, 2018.

Vandaele, A. C., Hermans, C., Simon, P. C., Carleer, M., Colin, R., Fally, S., Mérienne, M. F., Jenouvrier, A. and Coquart, B.: Measurements of the NO₂ absorption cross-section from 42000 cm⁻¹ to 10000 cm⁻¹ (238-1000 nm) at 220 K and 294 K, *Journal of Quantitative Spectroscopy and Radiative Transfer*, 59(3–5), 171–184, doi:10.1016/S0022-4073(97)00168-4, 1998.

Vaughan, M. A., Young, S. A., Winker, D. M., Powell, K. A., Omar, A. H., Liu, Z., Hu, Y. and Hostetler, C. A.: Fully automated analysis of space-based lidar data: an overview of the CALIPSO retrieval algorithms and data products, in *Laser Radar Techniques for Atmospheric Sensing*, vol. 5575, pp. 16–30, International Society for Optics and Photonics., 2004.

Veefkind, J. P., Aben, I., McMullan, K., Förster, H., de Vries, J., Otter, G., Claas, J., Eskes, H. J., de Haan, J. F., Kleipool, Q., van Weele, M., Hasekamp, O., Hoogeveen, R., Landgraf, J., Snel, R., Tol, P., Ingmann, P., Voors, R., Kruizinga, B., Vink, R., Visser, H. and Levelt, P. F.: TROPOMI on the ESA Sentinel-5 Precursor: A GMES mission for global observations of the atmospheric composition for climate, air quality and ozone layer applications, *Remote Sensing of Environment*, 120, 70–83, doi:10.1016/j.rse.2011.09.027, 2012.

Volkamer, R., Molina, L. T., Molina, M. J., Shirley, T. and Brune, W. H.: DOAS measurement of glyoxal as an indicator for fast VOC chemistry in urban air, *Geophysical Research Letters*, 32(8), n/a–n/a, doi:10.1029/2005GL022616, 2005a.

700 Volkamer, R., Spietz, P., Burrows, J. and Platt, U.: High-resolution absorption cross-section of glyoxal in the UV–vis and IR spectral ranges, *Journal of Photochemistry and Photobiology A: Chemistry*, 172(1), 35–46, doi:10.1016/j.jphotochem.2004.11.011, 2005b.

705 Volkamer, R., San Martini, F., Molina, L. T., Salcedo, D., Jimenez, J. L. and Molina, M. J.: A missing sink for gas-phase glyoxal in Mexico City: Formation of secondary organic aerosol, *Geophysical Research Letters*, 34(19), doi:10.1029/2007GL030752, 2007.

Vountas, M., Rozanov, V. V. and Burrows, J. P.: Ring effect: Impact of rotational Raman scattering on radiative transfer in earth's atmosphere, *Journal of Quantitative Spectroscopy and Radiative Transfer*, 60(6), 943–961, doi:10.1016/S0022-4073(97)00186-6, 1998.

710 Vrekoussis, M., Wittrock, F., Richter, A. and Burrows, J. P.: Temporal and spatial variability of glyoxal as observed from space, *Atmos. Chem. Phys.*, 9(13), 4485–4504, doi:10.5194/acp-9-4485-2009, 2009.

715 Vrekoussis, M., Wittrock, F., Richter, A. and Burrows, J. P.: GOME-2 observations of oxygenated VOCs: what can we learn from the ratio glyoxal to formaldehyde on a global scale?, *Atmos. Chem. Phys.*, 10(21), 10145–10160, doi:10.5194/acp-10-10145-2010, 2010.

Wittrock, F., Richter, A., Oetjen, H., Burrows, J. P., Kanakidou, M., Myriokefalitakis, S., Volkamer, R., Beirle, S., Platt, U. and Wagner, T.: Simultaneous global observations of glyoxal and formaldehyde from space, *Geophysical Research Letters*, 33(16), n/a–n/a, doi:10.1029/2006GL026310, 2006.

- Zhang, Y., Wang, X., Wen, S., Herrmann, H., Yang, W., Huang, X., Zhang, Z., Huang, Z., He, Q. and George, C.: On-road vehicle emissions of glyoxal and methylglyoxal from tunnel tests in urban Guangzhou, China, *Atmospheric Environment*, 127, 55–60, doi:10.1016/j.atmosenv.2015.12.017, 2016.
- 725 Zien, A. W., Richter, A., Hilboll, A., Blechschmidt, A.-M. and Burrows, J. P.: Systematic analysis of tropospheric NO₂ long-range transport events detected in GOME-2 satellite data, *Atmos. Chem. Phys.*, 14(14), 7367–7396, doi:10.5194/acp-14-7367-2014, 2014.

Unexpected long-range transport of glyoxal and formaldehyde observed from the Copernicus Sentinel-5 Precursor satellite during the 2018 Canadian wildfires

Leonardo M. A. Alvarado¹, Andreas Richter¹, Mihalis Vrekoussis^{1,2,4}, Andreas Hilboll¹, Anna B. Kalisz Hedegaard^{3,1}, Oliver Schneising¹, and John P. Burrows¹

¹Institute of Environmental Physics (IUP), University of Bremen, Bremen, Germany

²Center of Marine Environmental Sciences (MARUM), University of Bremen, Bremen, Germany

³Institute of Atmospheric Physics, German Aerospace Center (DLR), Oberpfaffenhofen-Wessling, Germany

⁴Energy, Environment, and Water Research Center, The Cyprus Institute, Nicosia, Cyprus

10 *Correspondence to:* Leonardo M. A. Alvarado (lalvarado@iup.physik.uni-bremen.de)

Abstract. Glyoxal (CHO.CHO) and formaldehyde (HCHO) are intermediate products in the tropospheric oxidation of the majority of Volatile Organic Compounds (VOC). CHO.CHO is also a precursor of secondary organic aerosol (SOA) in the atmosphere. CHO.CHO and HCHO are released from biogenic, anthropogenic, and pyrogenic sources. CHO.CHO and HCHO tropospheric lifetimes are typically considered to be short during the daytime at mid-latitudes (e.g. several hours), as they are rapidly removed from the atmosphere by their photolysis, oxidation by OH, and uptake on particles or deposition. At night and at high latitudes, tropospheric lifetimes increase to many hours or even days. Previous studies demonstrated that CHO.CHO and HCHO vertical column densities, VCDs, are well retrieved from space-borne observations using the differential optical absorption spectroscopy, DOAS. In this study, we present CHO.CHO and HCHO VCDs retrieved from measurements of the TROPOMI instrument, launched on the Sentinel-5 Precursor (S5P) platform in October 2017. We observe strongly elevated amounts of CHO.CHO and HCHO during the 2018 fire season in British Columbia, Canada, where a large number of fires occurred in August. CHO.CHO and HCHO plumes from individual fire hot-spots are observed in air masses travelling over distances of up to 1500 km, i.e. much longer than expected for the relatively short tropospheric lifetime expected for CHO.CHO and HCHO. Comparison with simulations by the particle dispersion model FLEXPART indicates that effective lifetimes of 20 hours and more are needed to explain the observations of CHO.CHO and HCHO if they decay in an effective first order process. FLEXPART used in the study calculates accurately the transport. In addition an exponential decay, in our case assumed to be photochemical, of a species along the trajectory is added. We have used this simple approach to test our assumption that the CHO.CHO and HCHO are created in the fires and then decay at a constant rate in the plume, as it is transported. This is clearly not the case and we infer that CHOCHO and HCHO are either efficiently recycled during transport, or continuously formed from the oxidation of longer-lived precursors present in the plume, or possibly a mixture of both. We consider the best explanation of the observed CHO.CHO and HCHO VCD in the

plumes of the fire is that they are produced by oxidation of longer-lived precursors, also released by the fire and present in the plume.

1 Introduction

Formaldehyde (HCHO) is produced in the oxidation of both methane (CH₄) and other Volatile Organic Compounds (VOC).
35 Glyoxal (CHO.CHO) is the smallest alpha-dicarbonyl formed in the oxidation of many VOC containing two or more carbon atoms. Although both CHO.CHO and HCHO, which are known as OVOC (Oxygenated Volatile Organic Compounds) have similar rates of reaction with the hydroxyl radical (OH) in the troposphere, the photolysis frequency of HCHO, which absorbs and is photolysed in the ultraviolet-A (UV-A), is significantly smaller than that of CHO.CHO, which absorbs in the blue. As a result, the atmospheric lifetime of HCHO is longer than that of CHO.CHO (Atkinson, 2000). Both species are
40 short-lived during daytime due to their rapid removal by photolysis and reaction with OH radicals (Atkinson, 2000; Volkamer et al., 2007). These processes are the major sinks of CHO.CHO and HCHO, contributing about 69% and 96%, respectively. The remaining part of HCHO is removed by deposition (4%), while for CHO.CHO, 22% are removed by SOA formation and 8% by deposition (Stavrakou et al., 2009a, c). Additionally, HCHO and probably also CHO.CHO during the
45 night are removed by reaction with nitrate (NO₃) radicals (Atkinson, 2000). CHO.CHO and HCHO play a key role in tropospheric chemistry because they act as temporary reservoirs releasing carbon monoxide (CO) and HO_x (OH and Hydroperoxyl, HO₂) free radicals, which participate in catalytic cycles creating and destroying tropospheric ozone (O₃).

The slant and vertical column densities of HCHO were first observed from space using measurements from the GOME instrument (e.g. Burrows et al., 1999, and references therein). These columns were later used to estimate the emission strength of precursor VOC (Palmer et al., 2003; Abbot et al., 2003). The simultaneous observation of CHO.CHO and HCHO
50 (Wittrock et al., 2006) enabled an improved assessment of atmospheric VOC levels and the knowledge of the ratio of CHO.CHO-to-HCHO (R_{GF}), (Vrekoussis et al., 2010), provides some differentiation of source types. Studies have used HCHO, partly in combination with CHO.CHO to estimate the biogenic isoprene emissions (Fu et al., 2007; Stavrakou et al., 2009a, b, c; Liu et al., 2012; Marais et al., 2012). This is the largest natural source of CHO.CHO (Guenther et al., 2006; Fu et al., 2007). The amount of biogenically emitted VOC depends on several factors including, amongst others, the plant species
55 and weather conditions (e.g. temperature and humidity) (Guenther et al., 2000). In urban and rural regions, there are also contributions to the amounts of CHO.CHO from human activities, such as from fossil fuel production, distribution and combustion: the largest anthropogenic source of VOC precursors of CHO.CHO being motor vehicle emissions due to either evaporation or incomplete combustion of fuel (Kansal, 2009). Globally, 55% of CHO.CHO is produced by biogenic precursors, while 27% are from anthropogenic and the remaining 18% from pyrogenic emissions (Stavrakou et al., 2009a).
60 Fires and vehicle exhausts are thought to be the only two sources, which directly emit CHO.CHO (Stavrakou et al., 2009a; Zhang et al., 2016).

In August 2018, unusually high temperatures caused severe drought in some areas of North America and resulted in the outbreak of many wildfires: the province of British Columbia (BC) in Canada was one of the most affected areas. The 2018 season is the worst on record, with 6826 fires being detected and an area of approximately 22500 km² of land burned (Natural Resources Canada, 2018). These fires emitted many different pollutants into the atmosphere, e.g. CO, NO_x, VOC, OVOC, O₃, SO₂, CO₂, HCHO, HONO, CH₃CO.O₂.NO₂ (PAN) and other toxic species as well as aerosols (Urbanski et al., 2018). During the transport of plumes from fires, photochemical transformation of emitted species occurs. Overall, polluted air is transported to regions where the plumes are dispersed. CHO.CHO and HCHO column amounts are observed by remote sensing from satellite using Differential Optical Absorption Spectroscopy (DOAS) on measurements of the radiances backscattered from the Earth's surface and atmosphere. The global maps of CHO.CHO and HCHO retrieved from SCIAMACHY, GOME-2, and OMI show enhanced CHO.CHO and HCHO over tropical rain forests but also over other regions with high isoprene emissions. In addition, hot-spots of CHO.CHO and HCHO from fire emissions can be detected over large wildfires (Wittrock et al., 2006; Vrekoussis et al., 2009, 2010; Lerot et al., 2010; Chan Miller et al., 2014; Alvarado et al., 2014; De Smedt et al., 2008, 2012, 2015, 2018).

In this study, we present novel observations of CHO.CHO and HCHO retrieved from the high spatial resolution observations of the instrument TROPOMI on board the S5P platform. On 7 August 2018, strongly elevated amounts of CHO.CHO and HCHO were observed over British Columbia and attributed to being predominantly from fires. Surprisingly, these elevated levels of CHO.CHO and HCHO were not limited to the vicinity of the fires. The fire plumes, which contain both CHO.CHO and HCHO remain visible for several days and appear to travel long distances from the sources. We have used forward simulations of atmospheric transport of air masses calculated using the FLEXPART model (Pisso et al., 2019). The simulations include an effective first order loss, which determines the mean effective lifetime of the tracer. Those tracers emitted over the fire hot-spots with long effective lifetimes reproduce best the evolution of the plumes of CHO.CHO and HCHO for most of the fire events, and thus provide estimates of the effective lifetimes of CHO.CHO and HCHO in the plumes, as is described in the sections below. The R_{GF} provides knowledge about their sources in the plume. CO and nitrogen dioxide, NO₂, have respectively longer and shorter lifetimes with respect to reaction with OH, and smoke and aerosol are also transported in the plumes from fires. Consequently the retrieved vertical column densities of CO and NO₂ from the TROPOMI instrument and true color images from VIIRS instrument on NPP, which measures near simultaneously with TROPOMI are used as complementary information in our interpretation of the apparent enhanced lifetime of CHO.CHO and HCHO in the plume.

90 **2 Methods**

2.1 CHO.CHO and HCHO observations

The Differential Optical Absorption Spectroscopy (DOAS) method has been successfully applied to retrieve atmospheric columns of trace gases having fingerprint narrow absorption bands in the solar spectral range from space-borne instruments (e.g. Burrows et al., 1999). As noted above, there are several studies describing retrievals of OVOC and their use for the
95 identification of VOC sources and their emissions (Burrows et al., 1999; Palmer et al., 2001; Wittrock et al., 2006; Kurosu et al., 2007; Vrekoussis et al., 2009, 2010; Lerot et al., 2010; De Smedt et al., 2008, 2012, 2015, 2018; Hewson et al., 2013; González Abad et al., 2015; Chan Miller et al., 2014; Alvarado et al., 2014, 2015). Algorithms for the retrieval of HCHO and CHO.CHO have been developed for measurements from the SCanning Imaging Absorption spectroMeter for Atmospheric CHartographY (SCIAMACHY) (Burrows et al., 1995; Bovensmann et al., 1999), the Ozone Monitoring Instrument (OMI)
100 (Levelt et al., 2006), and the second Global Ozone Monitoring Experiment on MetOp-A and -B (GOME2-A and-B) (Munro et al., 2016), which in combination provide a continuous dataset covering a period of more than 20 years. In this study, measurements from the TROPOMI instrument on board the Sentinel-5 Precursor (Veefkind et al., 2012) are used to retrieve atmospheric column amounts of CHO.CHO and HCHO. A brief instrument description and relevant details of the retrieval of CHO.CHO and HCHO are given below.

105 **2.2 The TROPOMI instrument**

The TROPospheric Monitoring Instrument (TROPOMI) onboard the Copernicus Sentinel-5 Precursor satellite was launched on 13 October 2017. It has a spectral range in the UV-VIS-NIR-SWIR covering wavelengths from 270 to 500 nm in the UV-VIS, from 675 to 775 nm in the NIR and in a SWIR band from 2305 to 2385 nm. These bands allow the observation of several relevant atmospheric species, including CHO.CHO, HCHO, NO₂ and CO. TROPOMI provides nearly global
110 coverage each day at a spatial resolution which in August 2018 was 3.5 km×7 km (7 km×7 km in the SWIR). The equator crossing time is 13:30 LT (ascending node). Similar to OMI, TROPOMI is a nadir-viewing imaging spectrograph, employing a two-dimensional CCD, one dimension collecting the spectral information, the other being used for the spatial information. The TROPOMI instrument on board the S5P satellite provides data since November 2017 (Veefkind et al., 2012).

115 **2.3 CHO.CHO retrieval from TROPOMI measurements**

In recent years, several improvements on the retrieval of CHO.CHO have been reported. In 2014, Chan Miller et al. (2014) and Alvarado et al. (2014) presented new CHO.CHO retrieval algorithms applied to OMI measurements. These studies, similar to previous studies on GOME-2A data, introduced approaches to reduce interference by other absorbers, such as liquid water and nitrogen dioxide (NO₂). In this study, an optimized retrieval algorithm for CHO.CHO was developed,

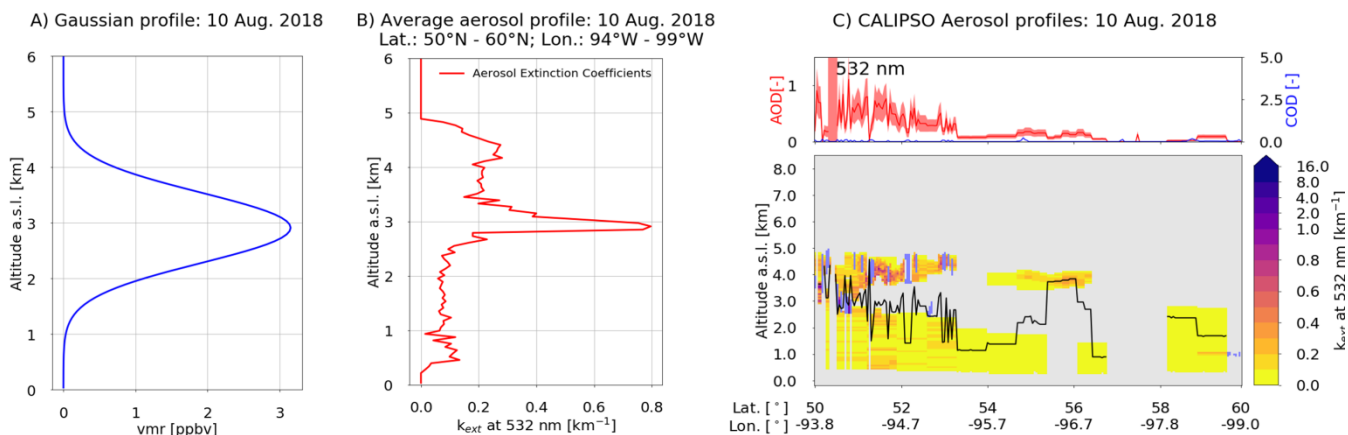
120 building on the heritage from the OMI CHO.CHO retrieval presented by Alvarado et al. (2014), extended and applied to S5P
measurements. Previous studies have shown that cross-correlations between references cross-sections, as well as
instrumental structures and shifts in the wavelength calibration can introduce systematic errors in the retrieval. As a result, a
strong dependence on the fitting window was identified in the retrieved CHO.CHO slant column densities, SCDs (Chan
Miller et al., 2014; Alvarado et al., 2014). In this study, a fitting window from 433 to 465 nm was chosen, which is slightly
125 larger than windows used in previous investigations (Vrekoussis et al., 2010; Alvarado et al., 2014). This fitting window,
which enables the liquid water absorption to be retrieved, leads to a reduction in the number of negative CHO.CHO SCDs
over oceanic regions in comparison to a shorter fitting window (e.g. 434–458 nm), as well as a reduction in the residuals.
The wavelength range selected covers the strong absorption bands of CHO.CHO (452–457 nm), which have already been
used in the past to retrieve CHO.CHO from ground and ship-based DOAS configurations as well as from satellites (Sinreich
130 et al., 2007, 2010; Wittrock et al., 2006; Vrekoussis et al., 2009, 2010; Lerot et al., 2010; Chan Miller et al., 2014; Alvarado
et al., 2014). In order to optimize the quality of the retrievals, a row-dependent daily mean Pacific spectrum from the region
50°S, 160°E – 50°N, 135°W is used as a background spectrum (Alvarado, 2016), which is computed by averaging over the
whole latitude range (50°S – 50°N) for each across-track viewing direction independently. In addition, the mean CHO.CHO
SCD over the region 30°S, 150°W – 30°N, 150°E is computed each day and subtracted from all SCDs to correct for possible
135 offsets. A summary of the selected absorption cross-sections, and other parameters used in the retrieval, as well as a list of
the species included in the retrieval, is shown in Table 1.

SCDs depend on observation geometry. VCDs are derived from the SCDs by use of so-called air mass factors (AMFs),
which depend on the trace gas profile, surface albedo, aerosols, clouds, and on solar zenith angle and measurement
geometry. As the focus of this study is the observation of CHO.CHO in biomass burning emissions, a simple CHO.CHO
140 profile with a Gaussian distribution having its maximum peak at the altitude of the aerosol layer is used (see Figure 1-A).
This is based on the assumption that CHO.CHO is found at the same location as the main plume of aerosol and other trace
gases. The altitude of the aerosol layer was estimated from profiles retrieved by the Cloud-Aerosol Lidar and Infrared
Pathfinder Satellite Observation (CALIPSO) (Vaughan et al., 2004) (Figure 1-B). These aerosol extinction coefficients (k_{ext})
profiles retrieved at 532 nm are also used in the calculation of the AMFs by the radiative transfer model SCIATRAN
145 (Rozanov et al., 2013). The computations have been performed on a daily basis, assuming a single scattering albedo of 0.92
and a homogenous distribution of aerosols characterized by the mean profile in the whole region of study. The latter is
computed from the average of all aerosol profiles taken over the region after removing cloud-contaminated pixels (see
Figure 1-C). Clouds are not explicitly accounted for in the CHO.CHO and HCHO retrievals but data are filtered for the
presence of clouds using an intensity criterion corresponding to a cloud radiance fraction of about 50%.

150

Table 1. Summary of retrieval parameters of CHO.CHO and HCHO from S5P with the respective absorption cross-sections used.

Parameters	Formaldehyde (HCHO)	Glyoxal (CHO.CHO)
Fitting window	323.5-361 nm	433-465 nm
Polynomial	5 coefficients	5 coefficients
Cross-sections used:		
HCHO (Meller and Mootgat, 2000)	Yes (298 K)	No
CHO.CHO (Volkamer et al., 2005)	No	Yes (296 K)
NO ₂ (Vandaele et al., 1998)	Yes (220 K)	Yes (220K, 2294 K)
O ₄ (Thalman et at., 2013)	Yes (293K)	Yes (293 K)
O ₃ (Serduchenko et al., 2014)	Yes (223 K, 243 K)	Yes (223 K)
BrO (Fleischmann et al., 2004)	Yes (223 K)	No
H ₂ O (Rothman et al., 2013)	No	Yes (296 K)
Liquid water (Mason et al., 2016)	No	Yes (280 K)
Ring effect	Ring cross section calculated by SCIATRAN model (Vountas et al., 1998)	
Non-linear ozone absorption effects, 2 pseudo absorption cross-sections ($O_3 * \lambda + (O_3)^2$) from Taylor expansion (Puķīte et al., 2010)	Yes	No
Iterative spike removal (Richter et al., 2011)	Applied	
Intensity offset correction	Linear offset (I/I ₀)	
Background spectrum	Pacific region (50° N, 135° W – 50° S, 160°)	

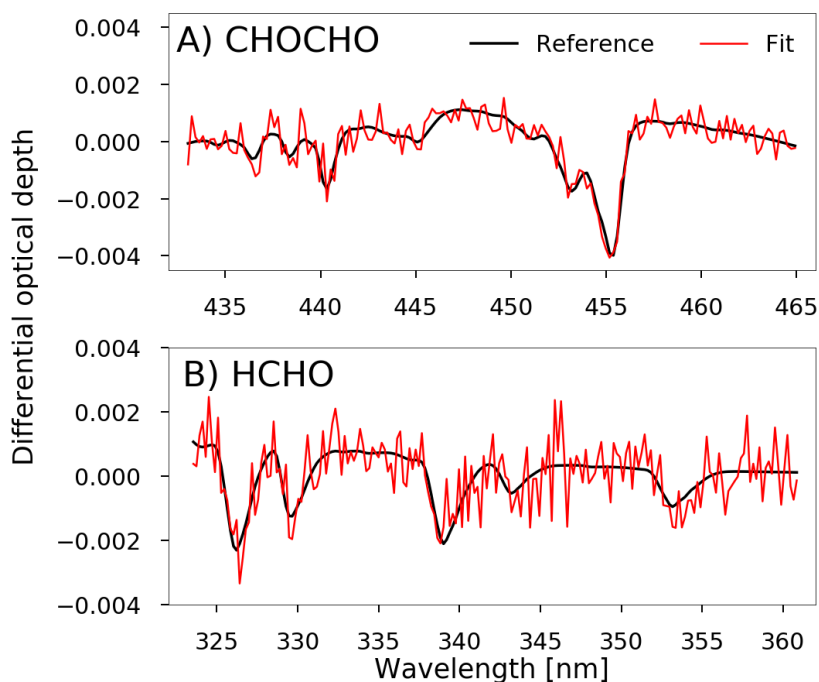


155 **Figure 1. A) CHO.CHO and HCHO profiles assumed in the computation of AMFs. B) CALIPSO profile of aerosol extinction coefficients (k_{ext}), averaged over for all latitudes and longitudes of Figure 1-C, excluding cloudy scenes. C) Top panel: Example of CALIPSO Aerosol profile extinction coefficients retrieved at a wavelength of 532 nm. Aerosol and cloud optical depth are shown as a function of latitude and longitude for every single profile. Bottom panel: Colour coded k_{ext} for every latitude and longitude in the selected region. Purple spots represent cloudy scenes. The black line depicts the aerosol layer height.**

160 2.4 HCHO retrieval from TROPOMI measurements

The accuracy of DOAS retrievals of HCHO is limited by cross-correlations with strong absorbers in the UV (e.g. O_3) and the signal to noise ratio of the radiance spectra measured by the instrument. Here, an updated and optimized version of the formaldehyde retrieval developed by Wittrock et al. (2006) and Vrekoussis et al. (2010) is used, which applies a slightly larger fitting window extending from 323.5 nm to 361 nm, resulting in a reduction in the noise of the retrieved slant column densities. At wavelengths shorter than 336 nm, interference with O_3 is observed due to the small optical depth of HCHO, which is about three orders of magnitude smaller. This effect is compensated by applying the method described by Pukite et al. (2010), which consists of adding two additional pseudo-cross-sections to the fit ($\lambda\sigma_{\text{O}_3}$ and $\sigma^2_{\text{O}_3}$) (Pukite et al., 2010; De Smedt et al., 2008, 2015, 2018). The cross-sections of interfering species are included in the fit as listed in Table 1. In a manner similar to the retrieval of CHO.CHO, a synthetic ring spectrum (Vountas et al., 1998) is used to account for the Ring effect and a row-dependent daily mean Pacific spectrum from the region 50°S , 135°W – 50°N , 160°E is used as background spectrum. A latitude dependent offset correction based on SCDs from longitudes between 180°E and 160°E is applied to the data. As for CHO.CHO, VCDs are computed using AMFs, assuming a Gaussian shape for the distribution of HCHO at the layer where the aerosols are located in the plume. Figures 2-A and 2-B show examples of CHO.CHO and HCHO fit results for 10 August 2018, compared to the differential reference cross-section for a single measurement. For an individual CHO.CHO measurement, the detection limit is of the order of 5×10^{14} molec. cm^{-2} , which is about 10 times smaller than the columns detected from emissions of the wildfires over the British Columbia region of Canada. For HCHO, the detection

limit is an order of magnitude higher (4.5×10^{15} molec.cm⁻²). The detection limit of a single S5P measurement in this study has been estimated in a manner similar to that explained in Alvarado et al. (2004).



180 **Figure 2.** A) Example fit for CHO.CHO from a single measurement of S5P taken at latitude 53.0° and longitude 125.6°W, on 10
August 2018 and for a solar zenith angle of 39.3°. B) Example fit for HCHO from a single measurement of S5P taken at latitude
59.1° and longitude 109.0° W, on 10 August 2018 and for a solar zenith angle of 44.6°. The black line depicts the scaled differential
cross-section and the red line the fit. The SCD values for this example are 9.3×10^{15} molec.cm⁻² for CHO.CHO and 4.6×10^{16}
185 4.5×10^{15} molec.cm⁻² for CHO.CHO and HCHO, respectively. The detection limit for a single measurement from S5P is estimated to be 5.0×10^{14} molec.cm⁻²
and 4.5×10^{15} molec.cm⁻² for CHO.CHO and HCHO, respectively.

2.5 Simulation of tracer transport with FLEXPART

In order to simulate the transport of emissions from the Canadian wildfires, forward simulations with version 10.3 of the
FLEXible PARTicle dispersion model FLEXPART (Stohl et al., 2005; Pisso et al., 2019) have been performed. The model
was driven by using hourly wind fields from the ECMWF ERA5 reanalysis (C3S) at 0.25° horizontal resolution. As a
190 transport model, FLEXPART does not simulate the complete set of chemical transformations leading to the observed
lifetimes of trace gases in the biomass burning plumes. However, performing simulations for tracers having different mean
lifetimes yields a valuable piece of information in order to understand the observed plume evolution. An effective mean
lifetime can be estimated by comparing the observed behaviour of the CHO.CHO and HCHO with FLEXPART simulations
of different assumed tracer lifetimes.

195 In FLEXPART, the effective mean lifetime τ of an emitted tracer is treated as exponential decay with a given half-life ($t_{0.5}$); τ can then be calculated according to $\tau = t_{0.5}/\ln(2)$. As part of this study, FLEXPART simulations were carried out with half-life times of 2, 4, 6, 8, 10, 12, 14, 16, 18, and 20 hours, corresponding to effective mean lifetimes of $\sim 2.9, 5.8, 8.7, 11.5, 14.4, 17.3, 20.2, 23.1, 26.0, \text{ and } 28.9$ hours, respectively. As emission rates from wildfires are highly uncertain, the emission fluxes from the Canadian wildfires are assumed to be proportional to fire radiative power (FRP, see below for more details).

200 The emissions, prescribed in the model, are taken from the Global Fire Assimilation System (GFAS) daily FRP and plume height data (Rémy et al., 2017). Simulations were performed on a daily basis for the period 6 to 23 August 2018. For each day, all fires from the GFAS data, which had an FRP of more than 3 W.cm^{-2} were gridded to a 0.350° horizontal pattern. The model was then run forward in time for 120 hours, releasing the tracer for the first 24 hours (the full UTC day) from each of the 0.350° grid cells, assuming no temporal variation throughout the day. Vertically, the emissions within the grid

205 cells were evenly distributed over the range of mean altitude of maximum injection heights given by the GFAS data for the respective grid cell. The output of the simulation contains gridded mass concentrations for each time step. Here, a grid with a horizontal resolution of 0.03125° was chosen, to match the resolution of the gridded satellite observations. Hourly output from the simulation was recorded and then vertically integrated to yield simulated tracer columns. In a post-processing step, for one specific mean lifetime, all simulation results (i.e., simulations for all fires on all days) were aggregated into one

210 dataset. While the absolute tracer column density from the model output cannot be simply compared to the measurements, a comparison of the plume patterns and relative distribution between satellite observation and model output gives an indication about the meaningfulness of the prescribed mean lifetime. At this point, the aggregated model output for one effective mean lifetime consists of hourly latitude-longitude grids of vertical tracer columns throughout the whole study period. For comparison to the satellite observations, the hourly time slice closest to the time of overpass at 53°N was chosen.

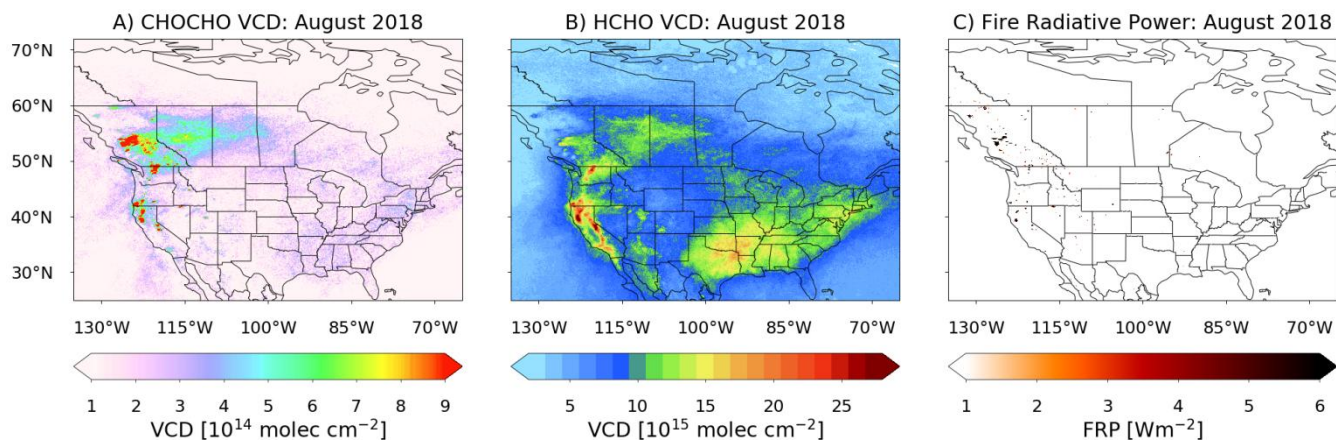
215 **3 Results and discussion**

During August 2018, a high-temperature anomaly led to the outbreak of many fires in the Canadian Western province of British Columbia, resulting in the emission of large quantities of particles and trace gases that in turn affected air quality in the region. As shown in Figure 3-A and -B, the monthly average of CHO.CHO and HCHO vertical columns from S5P show strongly enhanced values over the fire region, suggesting that these fires were a large direct and/or indirect source of

220 CHO.CHO and HCHO. Surprisingly, the CHO.CHO and HCHO enhancements are not limited to the main fire region but extend over large parts of Canada, where only a few fires were observed. In order to investigate the sources of CHO.CHO and HCHO and their distributions, 24-hour assimilation data of fire radiative power from the Global Fire Assimilation System (Kaiser et al., 2012) are analysed. Briefly, FRP is a measure of outgoing radiant heat from fires, measured in units of W.cm^{-2} and retrieved from space by the MODerate resolution Imaging Spectroradiometers (MODIS) on board of Terra and

225 Aqua satellites (Justice et al., 2002). The assimilated FRP spatially aggregates all valid fire and non-fire observations from

both MODIS instruments onto a horizontal resolution of $0.1^\circ \times 0.1^\circ$ and computes the total FRP sums for each grid bin (Justice et al., 2002). The FRP is also used as input in the FLEXPART simulation as described in section 2.5 as a proxy for emission strength. Figure 3-C shows a monthly average FRP map over North America for August 2018.



230

235

240

Figure 3. Monthly average of CHO.CHO (panel A) and HCHO (panel B) VCDs retrieved from the TROPOMI instrument on S5P for August 2018, and over North America (A and B). Panel C shows the integrated FRP from MODIS for the same period. The highest CHO.CHO VCD values are found over the locations of the most intense fires, as intuitively expected. The HCHO distribution over the fire regions is similar to that of CHO.CHO, but with some differences in the relative distribution. In addition, enhanced CHO.CHO and HCHO columns are also apparent over the south-eastern US, where large isoprene emissions occur. CHO.CHO and HCHO are also detected in plumes crossing central and eastern Canada, where no fires are identified in the FRP map. This pattern is best explained by the transport of CHO.CHO and HCHO emanating from the wildfires. However, CHO.CHO and HCHO have been reported to have short atmospheric lifetimes of about ~ 2.2 and ~ 4.0 hours during daytime, respectively (Atkinson, 2000; Volkamer et al., 2005a). Assuming that the lifetime in the plume is similar to that observed at the ground, we expect that CHO.CHO would be removed reasonably close to the fire sources. HCHO would be transported further but we would also expect that it would be transported no more than approximately twice as far as CHO.CHO.

245

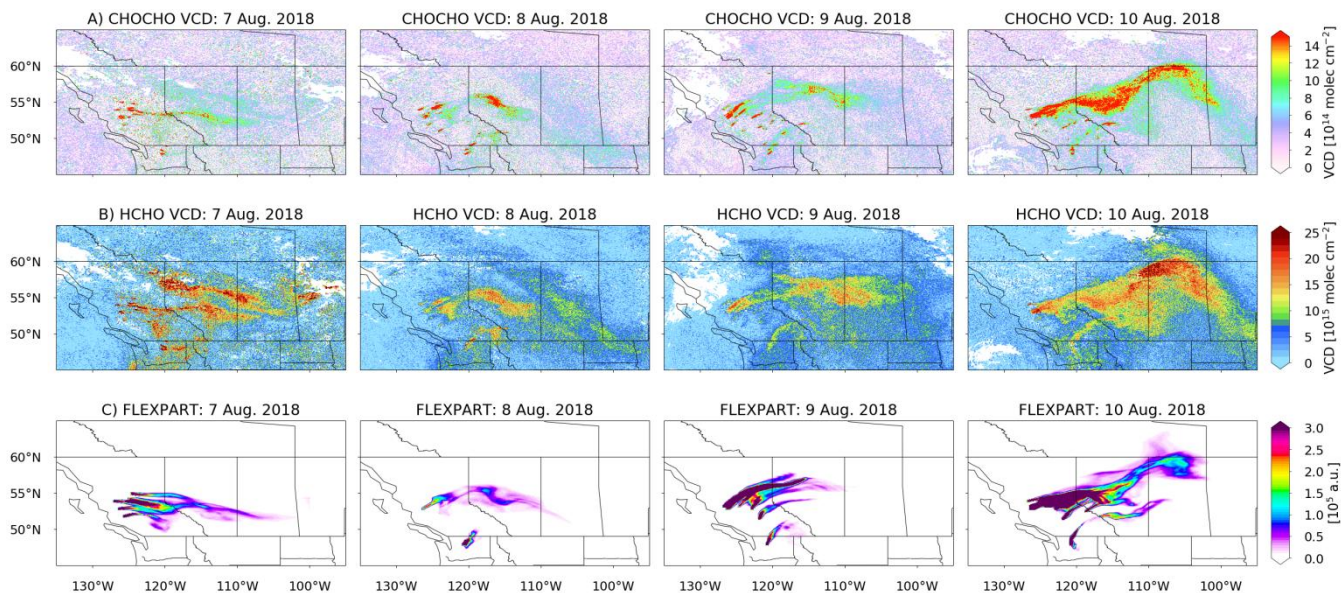
Earlier studies by Wittrock et al. (2006) and Vrekoussis et al. (2009, 2010) showed that CHO.CHO is also observed over oceanic regions, where no CHO.CHO source is expected. The potential of a) a long-range transport of CHO.CHO and/or of CHO.CHO precursors from continental areas, and b) having an unknown oceanic CHO.CHO source were discussed as a possible explanation in part of these observations, but no firm conclusions could be drawn so far. In the present study, with the support of the simulations using FLEXPART, evidence of long-range transport of CHO.CHO and HCHO or its

precursors from biomass burning emissions is investigated. In this context the transport of CHO.CHO and HCHO during two fire plume episodes from different periods (07-10 and 20-21 August 2018) are discussed below.

250 **3.1 CHO.CHO and HCHO emissions from the British Columbia wildfires: 07-10 and 20-21 August 2018**

Figure 4-A shows daily maps of CHO.CHO and HCHO VCDs over Canada for the period 7 to 10 August 2018. The most intense wildfires are found on 7 August 2018 and remain detectable until 10 August 2018. Both CHO.CHO and HCHO plumes are detected on the first day of the fire. The CHO.CHO and HCHO distributions then change from day to day. However, a large plume is clearly visible on 10 August 2018. Enhanced CHO.CHO and HCHO columns are found at a
255 distance of up to ~1500 km from the fires, indicating transport over long distances.

To investigate possible transport pathways, forward simulations of the atmospheric transport with FLEXPART were calculated for the period when CHO.CHO and HCHO plumes are observed (see Figure 4-B), assuming an effective lifetime of 14.4 hours. The latter is significantly longer than lifetimes of CHO.CHO and HCHO found in the literature. On the other hand, the simulated pattern of air masses follows the same distinctive path as CHO.CHO and HCHO VCDs. The tracer
260 simulated with FLEXPART spreads over the same area as CHO.CHO, providing evidence for the transport of CHO.CHO and HCHO and their precursors over continental Canada. This is more evident for the second period of interest in this study, which extends from the 20 to 21 of August 2018 (see Figure 7). While the spatial match of plume and model is good in this example, it is clear from the figure that an effective lifetime of 14.4 hours does not describe fully the extent of CHO.CHO and HCHO transported. Using shorter effective lifetimes for CHO.CHO and HCHO, taken from the literature would not
265 reproduce the observations. However both lifetimes depend on conditions in the plume: on the diurnal photolysis and OH diurnal cycles as well as on wet/dry deposition processes and other oxidants. Consequently, comparisons of FLEXPART simulations with different effective lifetimes were performed for two selected days, as is shown in Section 3.2.

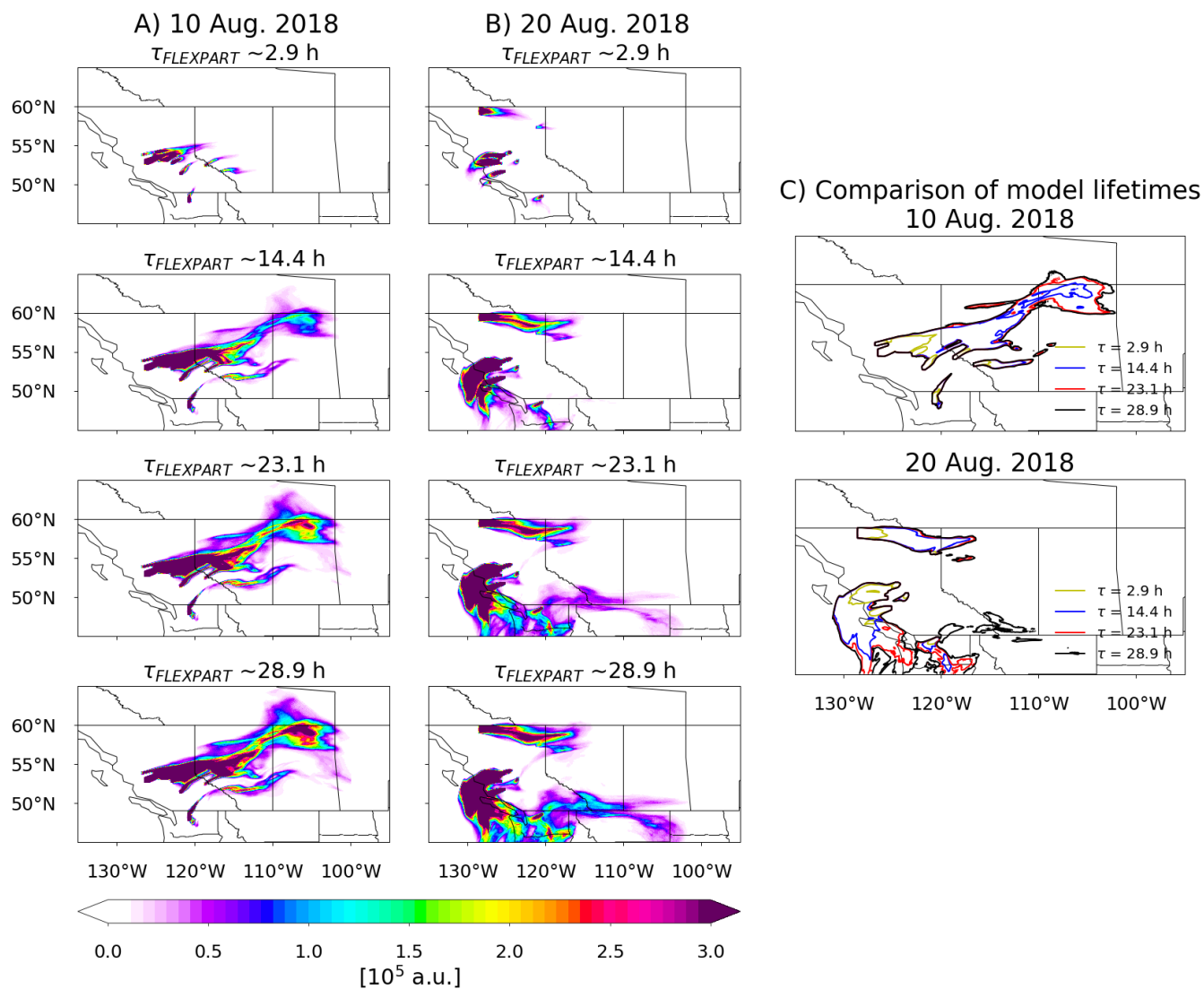


270 **Figure 4. A) and B) Daily CHO.CHO and HCHO VCDs retrieved from S5P measurements for the period 7 to 10 August 2018. C) Distribution of a tracer with a lifetime of 14.4 hours simulated with FLEXPART for the same period. The CHO.CHO in the plume decreases on average from 3×10^{15} molec.cm⁻² to 3×10^{14} molec.cm⁻², while the HCHO has a different variation in the plume but at the end of the plume, it decreases from 3×10^{16} molec.cm⁻² to 1×10^{16} molec.cm⁻². The FLEXPART tracer column decreases from 3×10^6 to 0.3×10^6 for this specific effective lifetime of 14.4 hours.**

3.2 Effective lifetimes of CHO.CHO and HCHO in the plume

275 Figure 5 shows the results of FLEXPART simulations assuming effective lifetimes for a surrogate chemical species of ~2.9, 14.4, 23.1, and 28.9 hours for 10 and 20 August 2018. From this figure, it is clear that only for the simulations having effective lifetimes of 23.1 hours or more, a significant fraction of the tracer emitted is present at the end of the plume as observed in the measurements. This is also illustrated in Figure 6, depicting CHO.CHO and HCHO maps for 10 August 2018. On top of these maps, contour lines are shown for the simulated air masses assuming effective lifetimes of ~2.9, 14.4, 280 and 28.9 hours. It is evident that in both cases the tracer distributions simulated with longer effective lifetimes better describe the observed distribution of CHO.CHO and HCHO.

Figures 7-A, -B, -C present a second comparison of daily maps of CHO.CHO and HCHO VCDs with a FLEXPART tracer having an effective lifetime of 28.9 hours for 20 and 21 August 2018. It is evident that again, the tracer follows the distribution of CHO.CHO and HCHO observations, similar to the first period studied (see Figure 4). However, on 20 and 21 285 August 2018, the CHO.CHO and HCHO plumes spread over the ocean, where no sources are expected, up to the point at which the plume disperses after being transported over a distance of about ~600 km from the fires.

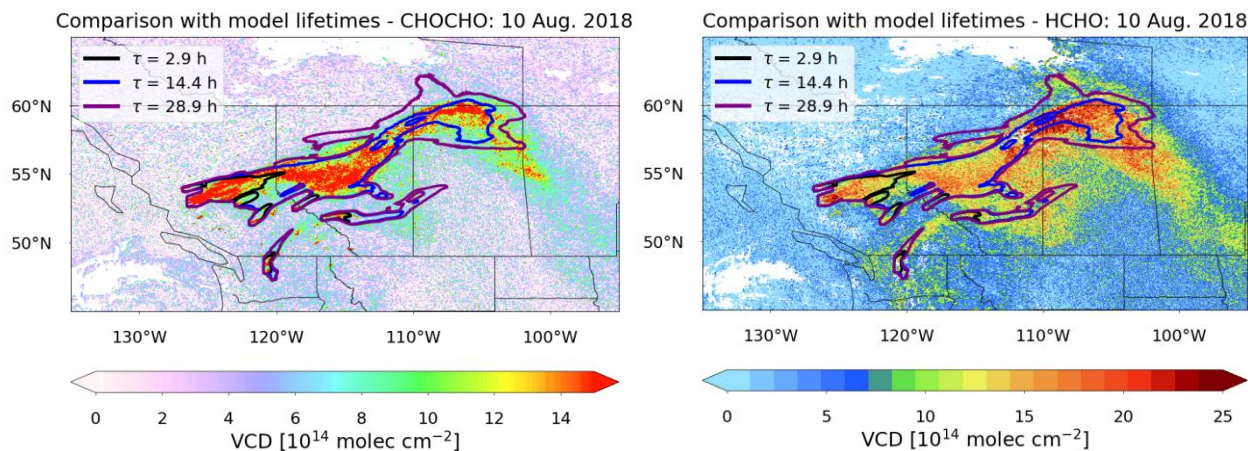


290 **Figure 5.** Daily maps of air masses simulated with FLEXPART for 10 and 20 August 2018 are shown (A and B) for selected effective lifetimes (~ 2.9 , 14.4, 23.1, 28.9 hours). C) Contour plots of simulations for the same lifetimes are compared for 10 and 20 August 2018.

The observed behaviour of the CHO.CHO and HCHO plumes is in contrast with the short atmospheric lifetimes resulting from their rapid removal by photolysis and reaction with OH. In addition, CHO.CHO oligomerises and thus is a source of SOA formation (Schweitzer et al., 1998; Jang et al., 2002; Liggió et al., 2005; Kroll et al., 2005; Loeffler et al., 2006; Volkamer et al., 2007; Fu et al., 2007; Myriokefalitakis et al., 2008; Stavrakou et al., 2009b, c). The simplest explanation of the observations of CHO.CHO and HCHO is that, during the fire events, both species are transported and/or produced during

295

transport over long distances, resulting in an effective lifetime of about 28.9 hours. This would imply the transport of VOC precursors of CHO.CHO and HCHO.



300 **Figure 6. Daily maps CHO.CHO and HCHO VCD retrieved from SSP for 10 August 2018 compared with FLEXPART tracer simulations having three different lifetimes (~2.9, 14.4, and 28.9 hours).**

One reason for the longer range transport of the CHO.CHO and HCHO plumes is the injection of the biomass burning emissions into the free troposphere, where high wind speeds favour transport over long distances. This is a well-known effect that has also been observed for NO₂ in GOME-2 data (Zien et al., 2014). However, even at high wind speeds, the short lifetime of these species would result in much smaller dispersed plumes than the ones observed. There are three possible explanations for this apparent contradiction:

305

Reason 1: The lifetimes of CHO.CHO and HCHO could be significantly longer than expected in these biomass burning plumes if the OH mixing ratio and UV and visible radiation within the plume are much lower than outside the plume. There is, however, no indication that this should be the case; on the contrary, OH levels in the biomass burning plume are expected to be enhanced (Folkens et al., 1997), leading to a reduction of the expected CHO.CHO and HCHO lifetimes. In this context, it is interesting to investigate the NO₂ VCD observed. The NO₂ plumes coming from the biomass burning are shown in figure 8-B. During daytime NO₂ is removed in the gas phase by reaction with OH. Provided sufficient O₃ is present the photolysis of NO₂ produces NO and O which react respectively with O₃ to make NO₂ and oxygen molecules to make O₃. This is known as a “do nothing cycle”. NO₂ appears to decay relatively rapidly in the plumes coming from the fires. Our assumption that oxidation and photolysis of CHO.CHO and HCHO is relatively rapid, is thus not contradicted by the NO₂ decay in the fire plumes.

315

Reason 2: There could be an efficient recycling process between the gas and aerosol phase, resulting in the observed extended effective lifetimes of CHO.CHO and HCHO. However, this reason is considered unlikely, because there is not yet

any strong evidence of HCHO being a precursor of SOA formation, and as the shape of the plumes for both trace gases is similar, a similar mechanism is expected for both. Also, evidence for the release of CHO.CHO following the formation of oligomers in the aerosol phase, is limited (Kroll et al., 2005, and references therein).

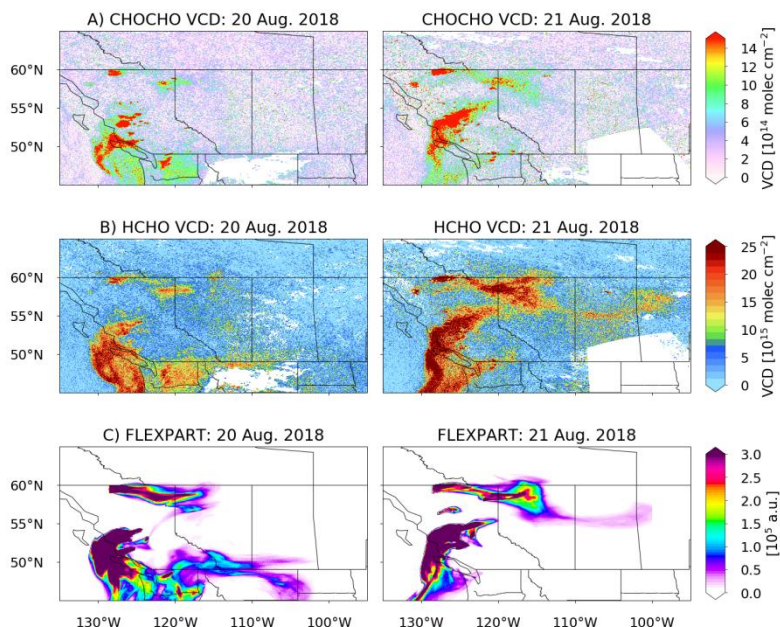


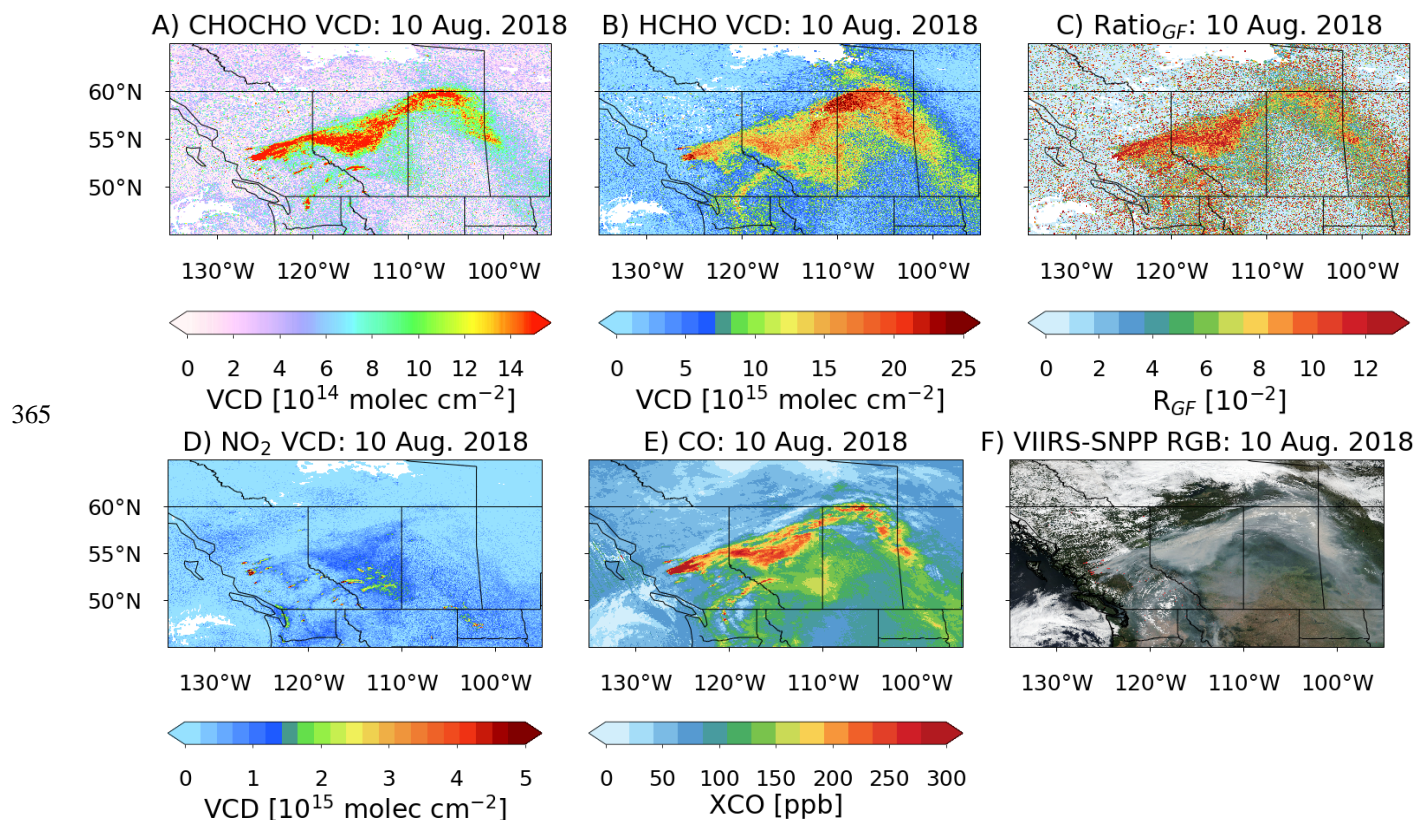
Figure 7. A) and B) Daily CHO.CHO and HCHO VCDs retrieved from S5P measurements for the period from 20 to 21 August 2018. C) Tracer distribution simulated with FLEXPART for the same period assuming a lifetime of 28.9 hours. Enhanced CHO.CHO columns spread over the ocean in a pattern similar to that simulated by the model tracer.

Reason 3: The plume could contain CHO.CHO and HCHO precursors, i.e. VOCs, which are slowly oxidized, releasing CHO.CHO and HCHO along the trajectory. If true, this would result in an apparent increase in lifetime. In order to better assess the CHO.CHO and HCHO spatial distribution seen on 10 August 2018, two additional TROPOMI retrievals have been taken into account; the column-averaged dry air mole fractions of CO, retrieved by the algorithm described in Schneising et al. (2019), and the NO₂ VCD retrieved using an algorithm similar to the one described for the GOME-2 instrument (Richter et al., 2011) and using AMF calculated following the same approach as the one described before for CHO.CHO and HCHO (see section 2.3). The CO plume shows a similar spatial pattern to those of CHO.CHO and HCHO (see Figure 8-E). As CO is a relatively long-lived tracer of fire emissions, having a lifetime with respect to OH of months, this supports the fire origin of the plume. As noted above, NO₂ is removed by OH faster than CHO.CHO and HCHO. The NO₂ VCD enhancements, in contrast to those of CHO.CHO and HCHO, are limited to the proximity of the fire hot spots (see Figure 8-D). This behaviour agrees with that assumed for a molecule with a short atmospheric lifetime. A true-colour image from the Visible Infrared Imaging Radiometer Suite (VIIRS) clearly shows the distribution of smoke and aerosols produced because of the emission from the fires being transported and transformed (Figure 8-F). The distribution of the aerosol

appears qualitatively to be similar to the CHO.CHO, HCHO, and CO distributions. We infer that the transported plumes are mixtures of CO, CHO.CHO, HCHO, aerosol and presumably other pollutants released by the fire. It is interesting to note that CHO.CHO and CO follow mainly the main plume, while the HCHO distribution is more diffuse and shows enhanced values also over regions where a thinner aerosol plume is visible in the VIIRS image. This may possibly originate from other unidentified fires or another unknown source, which is not included in our FLEXPART simulations.

As additional information, the ratio of CHO.CHO-to-HCHO, R_{GF} , is presented in Figure 8-C. Larger values of R_{GF} are found close to the location of the wildfires as already reported in previous publications (Vrekoussis et al., 2010). This is an indication of enhanced primary emissions of CHO.CHO relative to those of HCHO from fires. Lower R_{GF} values are found closer to the end of the plume implying a decreasing production of CHO.CHO relative to that of HCHO during the transport of polluted air in the plume. Another potential explanation would be the mixing in of air from different origins, having lower CHO.CHO and/or higher HCHO concentrations, during the plume transport. This is however not confirmed by the observed CO behaviour, which shows a similar spatial distribution to CHO.CHO and HCHO.

The comparison of retrieved S5P columns and FLEXPART tracer simulations discussed is based on a number of simplifications. The observational conditions of the biomass burning plumes are complex, and aerosol scattering and absorption impact on the sensitivity of the retrievals. While this is taken into account by using air mass factors for elevated plumes positioned at altitudes derived from CALIPSO observations, there remains considerable uncertainty with respect to absolute values. Aerosol loading and optical properties will vary along the plume and thus will the retrieval sensitivities. This not modelled explicitly in this study. However, the differences apparent between the spatial distributions of CHO.CHO and NO_2 , which are retrieved in similar spectral regions, provide evidence for the fact that measurement sensitivity does not explain the differences in the observed VCD plume patterns. Another crucial simplification is the assumption of a constant fire emissions and the proportionality of FRP and emission strength in the FLEXPART simulations. In reality, fire emissions will also depend on the type of biomass burned, the age of the fire, the time of the day and the environmental conditions, and this will have an effect on the trace gas distribution along the plume, which reflects both chemical transformation and the history of emissions. Modelling of this time-evolution is complex, if possible at all, and out of the scope of this study. However, the observation that both CHO.CHO and HCHO are present in the biomass burning plume after extended time periods and over long distances is robust and is best explained by the release of CHO.CHO and HCHO from the transformation of longer-lived precursors and/or efficient recycling processes in the plume as discussed above.



370 **Figure 8.** Panels A, B, D, and E show the CHO.CHO, HCHO, NO₂, and CO columns, respectively retrieved from S5P measurements for 10 August 2018. Note that CO columns are unfiltered and only represent a qualitative description of the plume. The AMFs used for CHO.CHO, HCHO, and NO₂ are appropriate for the biomass burning plume only. Panel C depicts the calculated CHO.CHO-to-HCHO (R_{GF}) for the same day. Panel F shows a true colour image of the aerosol distribution from VIIRS for 10 August 2018.

4 Summary and conclusions

375 The retrieval of CHO.CHO and HCHO VCDs from measurements of the TROPOMI instrument on board the Sentinel-5P satellite is reported. This will extend the datasets already available from the SCIAMACHY, GOME-2, and OMI instruments. The advantage of the high spatial resolution and low noise of TROPOMI for studying specific geophysical phenomena is well demonstrated in the features and plumes seen in the CHO.CHO, HCHO, CO, and NO₂ VCDs.

380 In this case study the satellite data show clear evidence for pyrogenic emissions of CHO.CHO and HCHO during the wildfire season in summer 2018 in British Columbia, Canada. The spatial and temporal pattern of the highest retrieved CHO.CHO and HCHO VCDs are associated with areas having high fire radiative power, as identified in the MODIS fire data products. This indicates that in these areas, pyrogenic emissions are the dominant source of CHO.CHO and HCHO. In

addition to local enhancements of NO₂, CHO.CHO, and HCHO, close to the fires, extended plumes of elevated CHO.CHO and HCHO VCD are observed downwind from the fires. This is in contrast with the behaviour of NO₂, which is also transported but is short lived. The spatial and temporal CHO.CHO and HCHO distribution observed from satellite follows a similar pattern to that of CO, which is long lived, and that simulated by the FLEXPART dispersion model, initialized by tracer emissions starting at known fire locations. Enhanced CHO.CHO and HCHO were found in the S5P data up to 1500 km from their sources.

In order to obtain reasonable agreement between the model results and the measurements, an effective tracer lifetime of more than 20 hours and up to 28.9 hours needs to be assumed in the FLEXPART simulations. This is significantly longer than the anticipated lifetimes of CHO.CHO and HCHO. The transport of CHO.CHO and HCHO along the length of the plume could be associated with these trace gases being lifted from the boundary layer into the free troposphere, where high wind speeds lead to rapid transport. The long apparent lifetime of CHO.CHO and HCHO in the transported plumes could be explained by a real increase in their lifetime in the plume because of photochemical conditions in the plume, which we consider unexpected. Based on our current knowledge, the most probable explanation of the apparent long lifetime of CHO.CHO and HCHO would be formation within the plume caused by the oxidation of a mixture of longer-lived emitted VOC precursors (e.g. methanol, ethanol, acetylene, aromatics, glycolaldehyde, ethylene etc.), that form CHO.CHO and HCHO at different rates. Further research is needed to investigate how frequent such fire-related long-range transport events of VOCs are. The chemical mechanism of the formation of the CHO.CHO and HCHO in the plumes downwind of the fires needs to be identified. The assessment of the number of such fires events and their relevance for tropospheric O₃ and aerosol production downwind of the fires and air quality is required.

400

Author contributions. L. M. A. Alvarado, A. Richter and J. P. Burrows have prepared the manuscript with the contribution of all authors and developed the glyoxal and formaldehyde and NO₂ retrievals for TROPOMI measurements. M. Vrekoussis, A. Hilboll and A. B. Kalisz Hedegaard have designed and performed the FLEXPART simulations of the airmasses assuming different effective lifetimes. O. Schneising has developed the CO retrieval and provided the CO data for the comparison with glyoxal and formaldehyde products.

Acknowledgements. The authors acknowledge financial support provided by the University of Bremen. Copernicus Sentinel-5P lv1 data from 2018 were used in this study. This publication contains modified COPERNICUS Sentinel data (2018). We thank the MACC team for providing the GFASv1.0 FRP and injection height products. FLEXPART simulations were conducted on the University of Bremen's HPC cluster Aether, funded by DFG within the scope of the Excellence Initiative.

VIIRS and CALIPSO data were obtained from the NASA Langley Research Center Atmospheric Science Data Center. FLEXPART simulation results were generated using Copernicus Climate Change Service Information (ERA5).

This is in part preparatory work for the analysis of the data from the DFG SPP HALO EMERGe project, which has one focus on biomass burning and the long range transport of such plumes. We thank Abram Sanders (European Organisation for the
415 Exploitation of Meteorological Satellites, Darmstadt) for providing support in the preparation of CALIPSO data for the computation of CHO.CHO and HCHO AMFs.

References

Abbot, D. S., Palmer, P. I., Martin, R. V., Chance, K. V., Jacob, D. J. and Guenther, A.: Seasonal and interannual variability of North American isoprene emissions as determined by formaldehyde column measurements from space, *Geophysical
420 Research Letters*, 30(17), doi:10.1029/2003GL017336, 2003.

Alvarado, L. M. A.: Investigating the role of glyoxal using satellite and MAX-DOAS measurements, PhD, University of Bremen., 2016.

425 Alvarado, L. M. A., Richter, A., Vrekoussis, M., Wittrock, F., Hilboll, A., Schreier, S. F. and Burrows, J. P.: An improved glyoxal retrieval from OMI measurements, *Atmos. Meas. Tech.*, 7(12), 4133–4150, doi:10.5194/amt-7-4133-2014, 2014.

Alvarado, L. M. A., Richter, A., Vrekoussis, M., Wittrock, F., Hilboll, A., Schreier, S. F. and Burrows, J. P.: Investigating the Link Between Glyoxal and Biogenic Activities, in *Towards an Interdisciplinary Approach in Earth System Science*,
430 edited by G. Lohmann, H. Meggers, V. Unnithan, D. Wolf-Gladrow, J. Notholt, and A. Bracher, pp. 59–65, Springer International Publishing., 2015.

Atkinson, R.: Atmospheric chemistry of VOCs and NO_x, *Atmospheric Environment*, 34(12–14), 2063–2101, doi:10.1016/S1352-2310(99)00460-4, 2000.

- 435 Behrens, L. K., Hilboll, A., Richter, A., Peters, E., Alvarado, L. M. A., Kalisz Hedegaard, A. B., Wittrock, F., Burrows, J. P. and Vrekoussis, M.: Detection of outflow of formaldehyde and glyoxal from the African continent to the Atlantic Ocean with a MAX-DOAS instrument, *Atmospheric Chemistry and Physics*, 19(15), 10257–10278, doi:<https://doi.org/10.5194/acp-19-10257-2019>, 2019.
- 440 Bovensmann, H., Burrows, J. P., Buchwitz, M., Frerick, J., Noël, S., Rozanov, V. V., Chance, K. V. and Goede, A. P. H.: SCIAMACHY: Mission Objectives and Measurement Modes, *Journal of the Atmospheric Sciences*, 56(2), 127–150, doi:10.1175/1520-0469(1999)056<0127:SMOAMM>2.0.CO;2, 1999.
- 445 Burrows, J. P., Hölzle, E., Goede, A. P. H., Visser, H. and Fricke, W.: SCIAMACHY—scanning imaging absorption spectrometer for atmospheric chartography, *Acta Astronautica*, 35(7), 445–451, doi:10.1016/0094-5765(94)00278-T, 1995.
- 450 Burrows, J. P., Weber, M., Buchwitz, M., Rozanov, V., Ladstätter-Weißmayer, A., Richter, A., DeBeek, R., Hoogen, R., Bramstedt, K., Eichmann, K.-U., Eisinger, M. and Perner, D.: The Global Ozone Monitoring Experiment (GOME): Mission Concept and First Scientific Results, *Journal of the Atmospheric Sciences*, 56(2), 151–175, doi:10.1175/1520-0469(1999)056<0151:TGOMEG>2.0.CO;2, 1999.
- Chan Miller, C., Gonzalez Abad, G., Wang, H., Liu, X., Kurosu, T., Jacob, D. J. and Chance, K.: Glyoxal retrieval from the Ozone Monitoring Instrument, *Atmos. Meas. Tech.*, 7(11), 3891–3907, doi:10.5194/amt-7-3891-2014, 2014.
- 455 De Smedt, I., Müller, J.-F., Stavrou, T., van der A, R., Eskes, H. and Van Roozendaal, M.: Twelve years of global observations of formaldehyde in the troposphere using GOME and SCIAMACHY sensors, *Atmos. Chem. Phys.*, 8(16), 4947–4963, doi:10.5194/acp-8-4947-2008, 2008.

De Smedt, I., Van Roozendael, M., Stavrakou, T., Müller, J.-F., Lerot, C., Theys, N., Valks, P., Hao, N. and van der A, R.:
460 Improved retrieval of global tropospheric formaldehyde columns from GOME-2/MetOp-A addressing noise reduction and
instrumental degradation issues, *Atmos. Meas. Tech.*, 5(11), 2933–2949, doi:10.5194/amt-5-2933-2012, 2012.

De Smedt, I., Stavrakou, T., Hendrick, F., Danckaert, T., Vlemmix, T., Pinardi, G., Theys, N., Lerot, C., Gielen, C.,
Vigouroux, C., Hermans, C., Fayt, C., Veefkind, P., Müller, J.-F. and Van Roozendael, M.: Diurnal, seasonal and long-term
465 variations of global formaldehyde columns inferred from combined OMI and GOME-2 observations, *Atmos. Chem. Phys.*,
15(21), 12519–12545, doi:10.5194/acp-15-12519-2015, 2015.

De Smedt, I., Theys, N., Yu, H., Danckaert, T., Lerot, C., Compernelle, S., Roozendael, M. V., Richter, A., Hilboll, A.,
Peters, E., Pedernana, M., Loyola, D., Beirle, S., Wagner, T., Eskes, H., Geffen, J. van, Boersma, K. F. and Veefkind, P.:
470 Algorithm theoretical baseline for formaldehyde retrievals from S5P TROPOMI and from the QA4ECV project,
Atmospheric Measurement Techniques, 11(4), 2395–2426, doi:https://doi.org/10.5194/amt-11-2395-2018, 2018.

Fleischmann, O. C., Hartmann, M., Burrows, J. P. and Orphal, J.: New ultraviolet absorption cross-sections of BrO at
atmospheric temperatures measured by time-windowing Fourier transform spectroscopy, *Journal of Photochemistry and*
475 *Photobiology A: Chemistry*, 168(1–2), 117–132, doi:10.1016/j.jphotochem.2004.03.026, 2004.

Folkens, I., Wennberg, P. O., Hanisco, T. F., Anderson, J. G. and Salawitch, R. J.: OH, HO₂, and NO in two biomass burning
plumes: Sources of HO_x and implications for ozone production, *Geophysical Research Letters*, 24(24), 3185–3188,
doi:10.1029/97GL03047, 1997.

480

Fu, T.-M., Jacob, D. J., Palmer, P. I., Chance, K., Wang, Y. X., Barletta, B., Blake, D. R., Stanton, J. C. and Pilling, M. J.:
Space-based formaldehyde measurements as constraints on volatile organic compound emissions in east and south Asia and
implications for ozone, *Journal of Geophysical Research: Atmospheres*, 112(D6), n/a–n/a, doi:10.1029/2006JD007853,
2007.

485

González Abad, G., Liu, X., Chance, K., Wang, H., Kurosu, T. P. and Suleiman, R.: Updated Smithsonian Astrophysical Observatory Ozone Monitoring Instrument (SAO OMI) formaldehyde retrieval, *Atmos. Meas. Tech.*, 8(1), 19–32, doi:10.5194/amt-8-19-2015, 2015.

490 Guenther, A., Geron, C., Pierce, T., Lamb, B., Harley, P. and Fall, R.: Natural emissions of non-methane volatile organic compounds, carbon monoxide, and oxides of nitrogen from North America, *Atmospheric Environment*, 34(12–14), 2205–2230, doi:10.1016/S1352-2310(99)00465-3, 2000.

Guenther, A., Karl, T., Harley, P., Wiedinmyer, C., Palmer, P. I. and Geron, C.: Estimates of global terrestrial isoprene
495 emissions using MEGAN (Model of Emissions of Gases and Aerosols from Nature), *Atmos. Chem. Phys.*, 6(11), 3181–3210, doi:10.5194/acp-6-3181-2006, 2006.

Hewson, W., Bösch, H., Barkley, M. P. and De Smedt, I.: Characterisation of GOME-2 formaldehyde retrieval sensitivity, *Atmos. Meas. Tech.*, 6(2), 371–386, doi:10.5194/amt-6-371-2013, 2013.

500

Jang, M., Czoschke, N. M., Lee, S. and Kamens, R. M.: Heterogeneous Atmospheric Aerosol Production by Acid-Catalyzed Particle-Phase Reactions, *Science*, 298(5594), 814–817, doi:10.1126/science.1075798, 2002.

Justice, C. O., Giglio, L., Korontzi, S., Owens, J., Morisette, J. T., Roy, D., Descloitres, J., Alleaume, S., Petitcolin, F. and

505 Kaufman, Y.: The MODIS fire products, *Remote Sensing of Environment*, 83(1–2), 244–262, doi:10.1016/S0034-4257(02)00076-7, 2002.

Kaiser, J. W., Heil, A., Andreae, M. O., Benedetti, A., Chubarova, N., Jones, L., Morcrette, J.-J., Razinger, M., Schultz, M. G., Suttie, M. and van der Werf, G. R.: Biomass burning emissions estimated with a global fire assimilation system based on
510 observed fire radiative power, *Biogeosciences*, 9(1), 527–554, doi:10.5194/bg-9-527-2012, 2012.

Kansal, A.: Sources and reactivity of NMHCs and VOCs in the atmosphere: A review, *Journal of Hazardous Materials*, 166(1), 17–26, doi:10.1016/j.jhazmat.2008.11.048, 2009.

515 Kroll, J. H., Ng, N. L., Murphy, S. M., Varutbangkul, V., Flagan, R. C. and Seinfeld, J. H.: Chamber studies of secondary organic aerosol growth by reactive uptake of simple carbonyl compounds, *J. Geophys. Res.*, 110(D23), D23207, doi:10.1029/2005JD006004, 2005.

Kurosu, T. P., Chance, K. and Volkamer, R.: Measurements of HCHO, CHOCHO, and BrO from the Ozone Monitoring
520 Instrument on EOS AURA, in *Proceedings of Envisat Symposium.*, 2007.

Lerot, C., Stavrakou, T., De Smedt, I., Müller, J.-F. and Van Roozendael, M.: Glyoxal vertical columns from GOME-2 backscattered light measurements and comparisons with a global model, *Atmos. Chem. Phys.*, 10(24), 12059–12072, doi:10.5194/acp-10-12059-2010, 2010.

525

Levelt, P. F., van den Oord, G. H. J., Dobber, M. R., Malkki, A., Visser, H., Vries, J. de, Stammes, P., Lundell, J. O. V. and Saari, H.: The ozone monitoring instrument, *IEEE Transactions on Geoscience and Remote Sensing*, 44(5), 1093 – 1101, doi:10.1109/TGRS.2006.872333, 2006.

530 Liggió, J., Li, S.-M. and McLaren, R.: Reactive uptake of glyoxal by particulate matter, *Journal of Geophysical Research: Atmospheres*, 110(D10), doi:10.1029/2004JD005113, 2005.

Liu, Z., Wang, Y., Vrekoussis, M., Richter, A., Wittrock, F., Burrows, J. P., Shao, M., Chang, C.-C., Liu, S.-C., Wang, H. and Chen, C.: Exploring the missing source of glyoxal (CHOCHO) over China, *Geophysical Research Letters*, 39(10),
535 doi:10.1029/2012GL051645, 2012.

- Loeffler, K. W., Koehler, C. A., Paul, N. M. and De Haan, D. O.: Oligomer Formation in Evaporating Aqueous Glyoxal and Methyl Glyoxal Solutions, *Environ. Sci. Technol.*, 40(20), 6318–6323, doi:10.1021/es060810w, 2006.
- 540 Marais, E. A., Jacob, D. J., Kurosu, T. P., Chance, K., Murphy, J. G., Reeves, C., Mills, G., Casadio, S., Millet, D. B., Barkley, M. P., Paulot, F. and Mao, J.: Isoprene emissions in Africa inferred from OMI observations of formaldehyde columns, *Atmos. Chem. Phys.*, 12(14), 6219–6235, doi:10.5194/acp-12-6219-2012, 2012.
- Mason, J. D., Cone, M. T. and Fry, E. S.: Ultraviolet (250–550 nm) absorption spectrum of pure water,
545 *Appl. Opt.*, AO, 55(25), 7163–7172, doi:10.1364/AO.55.007163, 2016.
- Meller, R. and Moortgat, G. K.: Temperature dependence of the absorption cross sections of formaldehyde between 223 and 323 K in the wavelength range 225–375 nm, *J. Geophys. Res.*, 105(D6), 7089–7101, doi:10.1029/1999JD901074, 2000.
- 550 Munro, R., Lang, R., Klaes, D., Poli, G., Retscher, C., Lindstrot, R., Huckle, R., Lacan, A., Grzegorski, M., Holdak, A., Kokhanovsky, A., Livschitz, J. and Eisinger, M.: The GOME-2 instrument on the Metop series of satellites: instrument design, calibration, and level 1 data processing – an overview, *Atmos. Meas. Tech.*, 9(3), 1279–1301, doi:10.5194/amt-9-1279-2016, 2016.
- 555 Myriokefalitakis, S., Vrekoussis, M., Tsigaridis, K., Wittrock, F., Richter, A., Brühl, C., Volkamer, R., Burrows, J. P. and Kanakidou, M.: The influence of natural and anthropogenic secondary sources on the glyoxal global distribution, *Atmos. Chem. Phys.*, 8(16), 4965–4981, doi:10.5194/acp-8-4965-2008, 2008.

Natural Resources Canada: Canadian Wildland Fire Information System | Archived reports, [online] Available from:
560 <http://cwfis.cfs.nrcan.gc.ca/report/archives?year=2018&month=08&day=29&process=Submit> (Accessed 12 April 2019),
2018.

Palmer, P. I., Jacob, D. J., Chance, K., Martin, R. V., Spurr, R. J. D., Kurosu, T. P., Bey, I., Yantosca, R., Fiore, A. and Li,
565 Q.: Air mass factor formulation for spectroscopic measurements from satellites: Application to formaldehyde retrievals from
the Global Ozone Monitoring Experiment, *Journal of Geophysical Research: Atmospheres*, 106(D13), 14539–14550,
doi:10.1029/2000JD900772, 2001.

Palmer, P. I., Jacob, D. J., Fiore, A. M., Martin, R. V., Chance, K. and Kurosu, T. P.: Mapping isoprene emissions over
North America using formaldehyde column observations from space, *Journal of Geophysical Research: Atmospheres*,
570 108(D6), n/a–n/a, doi:10.1029/2002JD002153, 2003.

Pisso, I., Sollum, E., Grythe, H., Kristiansen, N., Cassiani, M., Eckhardt, S., Arnold, D., Morton, D., Thompson, R. L., Groot
Zwaaftink, C. D., Evangeliou, N., Sodemann, H., Haimberger, L., Henne, S., Brunner, D., Burkhardt, J. F., Fouilloux, A.,
Brioude, J., Philipp, A., Seibert, P. and Stohl, A.: The Lagrangian particle dispersion model FLEXPART version 10.3,
575 *Geoscientific Model Development Discussions*, 1–67, doi:<https://doi.org/10.5194/gmd-2018-333>, 2019.

Puķīte, J., Köhl, S., Deutschmann, T., Platt, U. and Wagner, T.: Extending differential optical absorption spectroscopy for
limb measurements in the UV, *Atmos. Meas. Tech.*, 3(3), 631–653, doi:10.5194/amt-3-631-2010, 2010.

580 Rémy, S., Veira, A., Paugam, R., Sofiev, M., Kaiser, J. W., Marenco, F., Burton, S. P., Benedetti, A., Engelen, R. J., Ferrare,
R. and Hair, J. W.: Two global data sets of daily fire emission injection heights since 2003, *Atmospheric Chemistry and
Physics*, 17(4), 2921–2942, doi:<https://doi.org/10.5194/acp-17-2921-2017>, 2017.

- 585 Richter, A., Begoin, M., Hilboll, A. and Burrows, J. P.: An improved NO₂ retrieval for the GOME-2 satellite instrument, *Atmos. Meas. Tech.*, 4(6), 1147–1159, doi:10.5194/amt-4-1147-2011, 2011.
- 590 Rothman, L. S., Gordon, I. E., Babikov, Y., Barbe, A., Chris Benner, D., Bernath, P. F., Birk, M., Bizzocchi, L., Boudon, V., Brown, L. R., Campargue, A., Chance, K., Cohen, E. A., Coudert, L. H., Devi, V. M., Drouin, B. J., Fayt, A., Flaud, J.-M., Gamache, R. R., Harrison, J. J., Hartmann, J.-M., Hill, C., Hodges, J. T., Jacquemart, D., Jolly, A., Lamouroux, J., Le Roy, R. J., Li, G., Long, D. A., Lyulin, O. M., Mackie, C. J., Massie, S. T., Mikhailenko, S., Müller, H. S. P., Naumenko, O. V., Nikitin, A. V., Orphal, J., Perevalov, V., Perrin, A., Polovtseva, E. R., Richard, C., Smith, M. A. H., Starikova, E., Sung, K., Tashkun, S., Tennyson, J., Toon, G. C., Tyuterev, V. G. and Wagner, G.: The HITRAN2012 molecular spectroscopic database, *Journal of Quantitative Spectroscopy and Radiative Transfer*, 130, 4–50, doi:10.1016/j.jqsrt.2013.07.002, 2013.
- 595 Rozanov, V. V., Rozanov, A. V., Kokhanovsky, A. A. and Burrows, J. P.: Radiative transfer through terrestrial atmosphere and ocean: Software package SCIATRAN, *Journal of Quantitative Spectroscopy and Radiative Transfer*, doi:10.1016/j.jqsrt.2013.07.004, 2013.
- 600 Schneising, O., Buchwitz, M., Reuter, M., Bovensmann, H., Burrows, J. P., Borsdorff, T., Deutscher, N. M., Feist, D. G., Griffith, D. W. T., Hase, F., Hermans, C., Iraci, L. T., Kivi, R., Landgraf, J., Morino, I., Notholt, J., Petri, C., Pollard, D. F., Roche, S., Shiomi, K., Strong, K., Sussmann, R., Velasco, V. A., Warneke, T. and Wunch, D.: A scientific algorithm to simultaneously retrieve carbon monoxide and methane from TROPOMI onboard Sentinel-5 Precursor, *Atmospheric Measurement Techniques Discussions*, 1–44, doi:https://doi.org/10.5194/amt-2019-243, 2019.
- 605 Schweitzer, F., Magi, L., Mirabel, P. and George, C.: Uptake Rate Measurements of Methanesulfonic Acid and Glyoxal by Aqueous Droplets, *J. Phys. Chem. A*, 102(3), 593–600, doi:10.1021/jp972451k, 1998.
- 610 Serdyuchenko, A., Gorshchev, V., Weber, M., Chehade, W. and Burrows, J. P.: High spectral resolution ozone absorption cross-sections – Part 2: Temperature dependence, *Atmospheric Measurement Techniques*, 7(2), 625–636, doi:https://doi.org/10.5194/amt-7-625-2014, 2014.

Sinreich, R., Volkamer, R., Filsinger, F., Frieß, U., Kern, C., Platt, U., Sebastián, O. and Wagner, T.: MAX-DOAS detection of glyoxal during ICARTT 2004, *Atmos. Chem. Phys.*, 7(5), 1293–1303, doi:10.5194/acp-7-1293-2007, 2007.

615 Sinreich, R., Coburn, S., Dix, B. and Volkamer, R.: Ship-based detection of glyoxal over the remote tropical Pacific Ocean, *Atmos. Chem. Phys.*, 10(23), 11359–11371, doi:10.5194/acp-10-11359-2010, 2010.

Stavrou, T., Müller, J.-F., De Smedt, I., Van Roozendaal, M., van der Werf, G. R., Giglio, L. and Guenther, A.: Evaluating the performance of pyrogenic and biogenic emission inventories against one decade of space-based formaldehyde columns, *Atmos. Chem. Phys.*, 9(3), 1037–1060, doi:10.5194/acp-9-1037-2009, 2009a.

Stavrou, T., Müller, J.-F., De Smedt, I., Van Roozendaal, M., van der Werf, G. R., Giglio, L. and Guenther, A.: Global emissions of non-methane hydrocarbons deduced from SCIAMACHY formaldehyde columns through 2003–2006, *Atmos. Chem. Phys.*, 9(11), 3663–3679, doi:10.5194/acp-9-3663-2009, 2009b.

625

Stavrou, T., Müller, J.-F., De Smedt, I., Van Roozendaal, M., Kanakidou, M., Vrekoussis, M., Wittrock, F., Richter, A. and Burrows, J. P.: The continental source of glyoxal estimated by the synergistic use of spaceborne measurements and inverse modelling, *Atmos. Chem. Phys.*, 9(21), 8431–8446, doi:10.5194/acp-9-8431-2009, 2009c.

630 Stohl, A., Forster, C., Frank, A., Seibert, P. and Wotawa, G.: Technical note: The Lagrangian particle dispersion model FLEXPART version 6.2, *Atmospheric Chemistry and Physics*, 5(9), 2461–2474, doi:https://doi.org/10.5194/acp-5-2461-2005, 2005.

Thalman, R., Baeza-Romero, M. T., Ball, S. M., Borrás, E., Daniels, M. J. S., Goodall, I. C. A., Henry, S. B., Karl, T., Keutsch, F. N., Kim, S., Mak, J., Monks, P. S., Muñoz, A., Orlando, J., Peppe, S., Rickard, A. R., Ródenas, M., Sánchez, P.,

Seco, R., Su, L., Tyndall, G., Vázquez, M., Vera, T., Waxman, E. and Volkamer, R.: Instrument intercomparison of glyoxal, methyl glyoxal and NO₂ under simulated atmospheric conditions, *Atmos. Meas. Tech.*, 8(4), 1835–1862, doi:10.5194/amt-8-1835-2015, 2015.

640 Urbanski, S. P., Reeves, M. C., Corley, R. E., Silverstein, R. P. and Hao, W. M.: Contiguous United States wildland fire emission estimates during 2003–2015, *Earth System Science Data*, 10(4), 2241–2274, doi:https://doi.org/10.5194/essd-10-2241-2018, 2018.

Vandaele, A. C., Hermans, C., Simon, P. C., Carleer, M., Colin, R., Fally, S., Mérienne, M. F., Jenouvrier, A. and Coquart, 645 B.: Measurements of the NO₂ absorption cross-section from 42000 cm⁻¹ to 10000 cm⁻¹ (238-1000 nm) at 220 K and 294 K, *Journal of Quantitative Spectroscopy and Radiative Transfer*, 59(3–5), 171–184, doi:10.1016/S0022-4073(97)00168-4, 1998.

Vaughan, M. A., Young, S. A., Winker, D. M., Powell, K. A., Omar, A. H., Liu, Z., Hu, Y. and Hostetler, C. A.: Fully 650 automated analysis of space-based lidar data: an overview of the CALIPSO retrieval algorithms and data products, in *Laser Radar Techniques for Atmospheric Sensing*, vol. 5575, pp. 16–30, International Society for Optics and Photonics., 2004.

Veefkind, J. P., Aben, I., McMullan, K., Förster, H., de Vries, J., Otter, G., Claas, J., Eskes, H. J., de Haan, J. F., Kleipool, Q., van Weele, M., Hasekamp, O., Hoogeveen, R., Landgraf, J., Snel, R., Tol, P., Ingmann, P., Voors, R., Kruizinga, B., Vink, R., Visser, H. and Levelt, P. F.: TROPOMI on the ESA Sentinel-5 Precursor: A GMES mission for global 655 observations of the atmospheric composition for climate, air quality and ozone layer applications, *Remote Sensing of Environment*, 120, 70–83, doi:10.1016/j.rse.2011.09.027, 2012.

Volkamer, R., Molina, L. T., Molina, M. J., Shirley, T. and Brune, W. H.: DOAS measurement of glyoxal as an indicator for fast VOC chemistry in urban air, *Geophysical Research Letters*, 32(8), n/a–n/a, doi:10.1029/2005GL022616, 2005a.

660

Volkamer, R., Spietz, P., Burrows, J. and Platt, U.: High-resolution absorption cross-section of glyoxal in the UV–vis and IR spectral ranges, *Journal of Photochemistry and Photobiology A: Chemistry*, 172(1), 35–46, doi:10.1016/j.jphotochem.2004.11.011, 2005b.

665 Volkamer, R., San Martini, F., Molina, L. T., Salcedo, D., Jimenez, J. L. and Molina, M. J.: A missing sink for gas-phase glyoxal in Mexico City: Formation of secondary organic aerosol, *Geophysical Research Letters*, 34(19), doi:10.1029/2007GL030752, 2007.

Vountas, M., Rozanov, V. V. and Burrows, J. P.: Ring effect: Impact of rotational Raman scattering on radiative transfer in earth's atmosphere, *Journal of Quantitative Spectroscopy and Radiative Transfer*, 60(6), 943–961, doi:10.1016/S0022-670 4073(97)00186-6, 1998.

Vrekoussis, M., Wittrock, F., Richter, A. and Burrows, J. P.: Temporal and spatial variability of glyoxal as observed from space, *Atmos. Chem. Phys.*, 9(13), 4485–4504, doi:10.5194/acp-9-4485-2009, 2009.

675 Vrekoussis, M., Wittrock, F., Richter, A. and Burrows, J. P.: GOME-2 observations of oxygenated VOCs: what can we learn from the ratio glyoxal to formaldehyde on a global scale?, *Atmos. Chem. Phys.*, 10(21), 10145–10160, doi:10.5194/acp-10-10145-2010, 2010.

Wittrock, F., Richter, A., Oetjen, H., Burrows, J. P., Kanakidou, M., Myriokefalitakis, S., Volkamer, R., Beirle, S., Platt, U. 680 and Wagner, T.: Simultaneous global observations of glyoxal and formaldehyde from space, *Geophysical Research Letters*, 33(16), n/a–n/a, doi:10.1029/2006GL026310, 2006.

Zhang, Y., Wang, X., Wen, S., Herrmann, H., Yang, W., Huang, X., Zhang, Z., Huang, Z., He, Q. and George, C.: On-road vehicle emissions of glyoxal and methylglyoxal from tunnel tests in urban Guangzhou, China, *Atmospheric Environment*, 685 127, 55–60, doi:10.1016/j.atmosenv.2015.12.017, 2016.

Zien, A. W., Richter, A., Hilboll, A., Blechschmidt, A.-M. and Burrows, J. P.: Systematic analysis of tropospheric NO₂ long-range transport events detected in GOME-2 satellite data, *Atmos. Chem. Phys.*, 14(14), 7367–7396, doi:10.5194/acp-14-7367-2014, 2014.